REVIEW

Check for updates

Chemistry of magnetic covalent organic frameworks (MagCOFs): from synthesis to separation applications

Priya Yadav, [ID] [ab] Manavi Yadav, [ab] Rashmi Gaur, [a] Radhika Gupta, [ID] [a]
Gunjan Arora, [ID] [ac] Anju Srivastava, *[b] Anandarup Goswami, [ID] *[d]
Manoj B. Gawande [ID] [e] and Rakesh K. Sharma [ID] *[a]

Magnetic covalent organic frameworks (MagCOFs) represent a new class of emerging material, primarily employed in separation applications. Due to their attractive properties such as easy and cost-effective synthesis, high porosity, large surface area, strong $\pi-\pi$ interactions between COF shells and facile magnetic recovery, MagCOFs are being widely deployed in adsorption applications and exhibited high adsorption performance. This review emphasizes on the key advancements in the synthesis of MagCOFs and documents their potential in diverse separation applications including nitro explosive treatment, heavy metal ion adsorption and extraction of persistent organic pollutants, poly aromatic hydrocarbons and endocrine-disrupting chemicals, among others. In addition to offering up-to-date research outcomes in the field of separation science by utilizing MagCOFs, this article also highlights the challenges and possible solutions in this exciting developing area of research.

[a] *Green Chemistry Network Centre, Department of Chemistry, University of Delhi, Delhi 110007, India. E-mail: rksharmagreenchem@hotmail.com*
[b] *Department of Chemistry, Hindu College, University of Delhi, Delhi 110007, India. E-mail: dr.anjusrivastava@gmail.com*
[c] *Department of Chemistry, Hansraj College, University of Delhi, Delhi 110007, India*
[d] *Chemistry Division, Department of Sciences and Humanities, Vignan's Foundation for Science, Technology and Research (VFSTR), Vadlamudi, Guntur 522 213, Andhra Pradesh, India*
[e] *Department of Industrial and Engineering Chemistry, Institute of Chemical Technology, Mumbai-Marathwada Campus, Jalna, Maharashtra, India*

Priya Yadav is an active member of Green Chemistry Network Centre, University of Delhi, India, and ACS. She received her BSc degree from University of Rajasthan, Jaipur in 2013 and MSc degree from Banasthali Vidyapith, Rajasthan in 2016. She is currently working at the Green Chemistry Network Centre. She has received the award for junior research fellowship from University Grants Commission, Delhi, India. She has numerous publications in renowned journals of RSC, ACS and Wiley. Her research interest includes fabrication of core–shell structured magnetic nanocatalysts and their applications in diverse organic transformations.

Priya Yadav

Radhika Gupta is currently pursuing her doctoral studies under the supervision of Professor R. K. Sharma at Green Chemistry Network Centre, University of Delhi, India. She received her Master's degree in Chemistry from Indian Institute of Technology, Delhi in 2015 and Bachelor's degree in Chemistry from Hansraj College, University of Delhi in 2013 where she also secured first position. She is presently serving as the Vice-Chair of ACS International Student Chapter University of Delhi. Her area of research includes green chemistry, catalysis through hydrogen bonding interactions, immobilization of ionic liquids and fabrication of magnetic nanocatalysts for various organic transformations.

Radhika Gupta

1. Introduction

Over the decades, porous materials have gained tremendous attention due to their magnificent potential and broad range of applications in the field of sensing, energy storage, catalysis, energy conversion, gas storage and separation, optoelectronics, *etc.*[1–3] To date, a variety of highly porous materials having large surface area such as hyper-cross-linked polymers, conjugated microporous polymers and polymers with intrinsic micro-porosity have been designed.[1] However, their linking chemistry and the subsequent product formation primarily relies on the kinetically controlled irreversible coupling reactions and unfortunately this irreversibility results in poor self-healing ability, structural disorder and formation of non-separable oligomers,

limiting their wider applicability. To overcome these challenges, organic porous polymers with long range ordered structure and high crystallinity are considered to be potential replacements.[4,5] In this context, the pioneering work by Prof. Omar Yaghi and co-workers first introduced covalent organic frameworks (COFs) in 2005 as a new generation of crystalline framework materials.[6–8]

COFs represent a promising class of well-defined porous and crystalline polymeric materials synthesized *via* condensation reactions of 2D and 3D organic building precursors.[9,10] In general, they are composed of light elements such as hydrogen, boron, oxygen, carbon, nitrogen and silicon which are linked *via* strong covalent bonds in a reversible manner to generate reticular architecture. This thermodynamically controlled and

Gunjan Arora

Gunjan Arora was born in India in the year 1992. She received her graduate degree in Chemistry in 2013; and post graduate degree specialized in Inorganic Chemistry in 2015 from Hansraj College, University of Delhi, India. She then joined Prof. Sharma's group to pursue her doctoral studies. She is currently a senior research fellow and an active member of Green Chemistry Network Centre, Department of Chemistry, University of Delhi, India. She is working in the area of Green Chemistry and Nanocatalysis. Her research interest includes the design and development of sustainable magnetically retrievable heterogeneous catalysts for various organic transformations.

Anju Srivastava

Prof. Anju Srivastava is a Professor of Chemistry and Principal of a premier institution ranked amongst top three in the country, Hindu College, University of Delhi. She received her MSc and PhD in Synthetic Polymer Chemistry from IIT Delhi and has a teaching experience of 24 years in subject areas of organic chemistry, biochemistry, environment chemistry and analytical chemistry. Following that she is co-editor of several books and has been nominated as Fellow at ILLL (Institute of Lifelong Learning) University of Delhi and conferred with the 'Distinguished Teacher' Award by Former President of India, Dr A. P. J. Abdul Kalam.

Anandarup Goswami

Dr Anandarup Goswami completed his BSc with Chemistry Hons. in 2002 from Presidency College, Kolkata, India and obtained his MSc in 2004 from Indian Institute of Technology, Kanpur, India. He then went on to receive his PhD from Cornell University, New York, USA and then undertook a few postdoctoral stints in USA, Europe, Czech Republic and then joined Vignan's Foundation for Science, Technology and Research (VFSTR) as Associate Professor in the Division of Chemistry, Department of Sciences and Humanities in November 2016. His main research area focuses on synthesis, characterization, and applications of nanomaterials in catalysis, environmental remediation, etc.

Manoj B. Gawande

Prof. Manoj B. Gawande received his PhD in 2008 from Institute of Chemical Technology, Mumbai, India, and then undertook several research stints in Germany, South Korea, Portugal, Czech Republic, USA, and UK. Presently, he is an Associate Professor at Institute of Chemical Technology, Mumbai-Marathwada Campus, India. Recently, he was invited as visiting professor in chemistry at RCPTM-CATRIN, Palacky University, Czech Republic. His research interests focus on single-atom catalysts, advanced nanomaterials, as well as cutting-edge catalysis and energy applications. He is also included in the global list of the top 2% of scientists in the chemistry field for the years 2019 and 2020 by Stanford University, US.
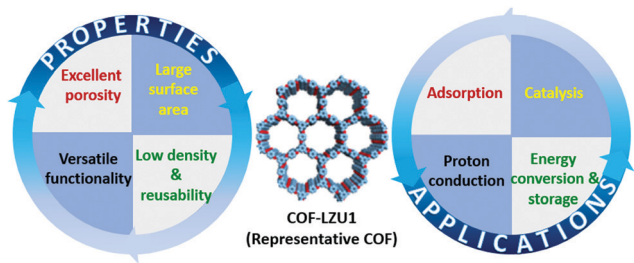
Fig. 1 Properties and applications of COFs.

reversible dynamic covalent chemistry of COFs allows "proof reading" and "error checking" during the synthesis and results into the self-healing ability of COFs leading to the formation of long range ordered crystalline structures.[11] Additionally, the presence of π–π interactions and hydrogen bonding among COF shells strengthens their porous skeleton and provides long-term stability.[3] Recently, COFs have attracted researchers' interest because of their intriguing properties such as tuneable composition and high thermal and chemical stability (Fig. 1)[12,13] and have been widely used in a variety of applications including energy conversion[14,15] and storage,[16,17] gas storage,[18,19] catalysis,[20–25] optoelectronics,[26,27] sensing,[28,29] drug delivery[30–32] and adsorption[33–35] to name a few.

Despite being recognized as a very promising class of materials at an early stage of discovery of COFs, unfortunately, the progress in the field is restricted due to some challenges. For example, their extraction from the matrix is not very efficient because of their low density which causes difficulty in their separation from reaction medium.[36] In addition, their large-scale applications are hampered due to tedious centrifugation and filtration methods. Over the past few decades, several techniques have been introduced to circumvent those challenges such as liquid–liquid phase extraction, Solid-phase extraction, solid-phase micro extraction, Soxhlet extraction and many others.[37] However, most of these techniques are often

associated with numerous shortcomings, including large amount of toxic solvent consumption, low selectivity, cumbersome filtration and time-consuming procedures.[38] Therefore, there is always a need to develop simple, environmentally benign and highly sensitive synthetic techniques which not only provide COFs with greater selectivity but also speed up the recovery process. Recently, magnetic solid-phase extraction (MSPE), a promising modification of SPE, has been developed as the most prominent technique in the field of separation and sample pre-treatment as it offers an easy recovery of adsorbent using a simple external magnetic field, with high extraction efficiency and large adsorption capacity.[39,40] Owing to the appealing properties of magnetic nanoparticles (e.g. Fe_3O_4; MNPs) including cost-effectiveness, reusability, easy operation, facile synthesis, low toxicity and good magnetic performance, they have been further explored in a variety of disciplines and are commonly used as magnetic extraction materials.[41–55] Moreover, a wide variety of functional moieties can be grafted over the surface of magnetic nanocomposites, which make further modifications and reactions more convenient. The introduction of magnetism in COFs has proven to be an effective strategy to solve the recovery problem of COFs. Considering the broad diversity, unique capability and wide applications of both magnetic nanoparticles and COFs, we believe that this combination will open up newer avenues in the rational design of core–shell structures with magnetic platforms and tuneable porous COF shells for wide applications.

Henceforth, after witnessing the effectiveness of MSPE, one of the notable approaches to circumvent the issue of separation would be to simultaneously integrate COFs with a magnetic component which would provide the ease of separation. This would give rise to MagCOFs that would combine the merits of rapid separation with adequate binding sites and high adsorption performance with enhanced functionality.[38,56–66] More recently, MagCOFs have marked a breakthrough in the current area of COF-related research. In particular, solid spherical magnetic core can offer a center for uniform COF growth and crystallization in all directions, which provides a possibility for controllable synthesis of magnetic core–shell COFs.[67] Therefore, synthesis of MagCOFs and the investigation of their in-depth utility in adsorption science has become an area of prime significance in material science.

1.1 Magnetic properties of MagCOF

MagCOF composites possess various significant features that are beneficial from green chemistry and sustainability viewpoints such as effortless and economic recovery. The evaluation of magnetic properties of the material is highly substantial. The magnetic properties of MagCOF are investigated using vibrating sample magnetometry (VSM) at room temperature.[68] In the hysteresis loop, to examine the magnetism, saturation magnetization (M_s) is used. Also, if no hysteresis loop and coercivity or remanence is observed in the curve, it suggests that MagCOF composites are superparamagnetic in nature.[69] It is shown that upon modification of MNPs with COF layer, saturation magnetization value of MagCOF composite decreases than initial MNPs.[70]

Dr R. K. Sharma is a professor and coordinator of Green Chemistry Network Centre at University of Delhi, India. He is also an Honorary Professor at Deakin University, Australia. He went to the University of Tokyo and Kumamoto University on JSPS Post-Doctoral Fellowship. He has published numerous book chapters, reviews and research articles in renowned international journals. He has also written/edited various books on Green Chemistry published by RSC, World Scientific and Wiley. Dr Sharma is also the Honorary Secretary of the RSC (North India Section) and faculty advisor of ACS International Student Chapter University of Delhi. http://greenchem.du.ac.in/.

Rakesh K. Sharma

Table 1 Saturation magnetization values and reusability runs of various MagCOFs

S. No.	MagCOF	Saturation magnetization (M_s)	Recyclability runs	Ref.
1	Fe$_3$O$_4$@COF	62.5	3	148
2	Fe$_3$O$_4$@TpBd	22	5	67
3	Fe$_3$O$_4$@COF	42.7	12	70
4	Magnetic TpPa-1	40.1	n.d.	71
5	Fe$_3$O$_4$@COF	48.4	10	100
6	M-COF-2	15.8	5	149
7	Fe$_3$O$_4$@COF	42	20	114
8	Fe$_3$O$_4$@COF@Au-β-CD	21.86	n.d.	150
9	MagCOF@MIP@CD	10.97	8	151
10	COF-(TpBd)/Fe$_3$O$_4$	51.8	4	142
11	SPIO@COF-guanidyl	42	5	121
12	Fe$_3$O$_4$@iCOFs	21.8	7	122
13	Fe$_3$O$_4$@SiO$_2$@TpPa-Ti^{4+}	35.67	n.d.	123
14	mTpBd-Me$_2$	60.5	5	152
15	M-DAPS-COF-SH	19.6	5	131
16	Fe$_3$O$_4$@COF(TpPa-1)	19.5	5	153
17	Fe$_3$O$_4$@COF(TpBD)@Au-MPS	40.7	n.d.	154
18	Fe$_3$O$_4$@TbBd	41.4	10	155

n.d. = no data.

Inspite of the decrease in M_s values of MagCOF, the synthetic material could be easily recovered from the reaction medium with the aid of an external magnet within few seconds.

Reusability and recyclability are the prime features of magnetic composites that controls the economy and efficiency of process at industrial scale. Although the benefits of using COFs as adsorbents are enormous, but their large-scale utility is still hampered due to their expensiveness, cumbersome filtration and centrifugation process used for the recovery of the composite. In this regard, MNPs supported COFs have been utilized as significant adsorbents for environmental remediation. This introduction of magnetism in COFs circumvent the issue of separation and provide the ease of separation.

To check the recyclability of MagCOF composite, numerous adsorption–desorption cycles are performed. In view of this, Cai *et al.* synthesized magnetic adsorbent (Fe$_3$O$_4$@COFs) and shows excellent stability and reusability even after ten adsorption–desorption cycles.[71] Similarly, Li and co-workers utilized Fe$_3$O$_4$@COF@Zr^{4+} for the extraction and determination of organophosphorus pesticides in vegetables.[72] Subsequently, various adsorption–desorption cycles were performed using the same magnetic composite. It is noteworthy that, prior to next cycle the as-synthesized MagCOF was washed with acetone and distilled water. Thus, Fe$_3$O$_4$@COF@Zr^{4+} can be reused for six cycles without any significant loss in its activity. Hence, the above examples state that MagCOF composite showed admirable reusability, mechanical stability and cost-effectiveness and also advantageous from environmental viewpoints. Table 1 lists the recyclability runs of numerous MagCOFs composites.

2. Focus of the review

In the present review, we focus on the synthesis of MagCOFs and their utility as magnetic extractants in various fields in combination with MSPE. The main insights of the review article are based on the development of MagCOFs in the domain of adsorption and separation, reflecting the need for their immobilization and deliberating the ways by which the immobilized MagCOFs can be fabricated. We have broadly discussed the adsorption of substances of concern for human health and environment such as endocrine-disrupting chemicals (EDCs), enrichment of phosphopeptides, nitro explosives and persistent organic pollutants (POPs), among others. The adsorption mechanism mainly lies on the strong π–π interactions, hydrophobic effect, electrostatic interaction and hydrogen bonding between aromatic rings of MagCOFs and phenyl rings of analytes. In recent years, numerous review articles have been documented in the literature on COFs and many research groups worldwide have explored the synthesis and applications of COFs.[2,3,12,73] The literatures accumulated on COFs are primarily focussed on (i) the current state-of-the-art on design, synthetic strategies, structural studies (structure of 2D and 3D COFs) and applications of COFs,[1] (ii) the development of heterogeneous single-site catalysts,[74] (iii) special emphasis has been given on the application of COFs in various fields such as catalytic, electrocatalytic, photocatalytic and separation applications (water treatment or the separation of gas mixtures and organic molecules, including chiral and isomeric compounds)[3,11,12] and (iv) a detailed description on shape/size selectivity as well as Schiff-base chemistry of COFs.[7] Numerous significant research articles have been published on synthesis of MagCOFs and their utility in separation applications.[60,67,69,71,75,76] The present review article consolidates the synthetic and applicative aspects of MagCOFs where MNPs immobilized COFs have been used for the extraction and separation of various analytes for analytical determinations of substances of concern areas.

3. Applications of magnetic COFs

As mentioned earlier, there is a need for sensitive and selective adsorption of inorganic and organic substances for a range of applications such as environmental monitoring, food quality control and chemical threat detection. Amongst a variety of adsorbents that have been designed and utilized in the past, MagCOFs based magnetic adsorbents have paved their own way on the account of their superior characteristics over others. Recently, several researchers have begun exploring the potential of MagCOFs as extraction materials due to their exceptional structural tunability and properties.[67] Described below, is a series of MagCOFs based chemical adsorbents that have been fabricated for the selective and efficient extraction of toxic chemical pollutants.

3.1 Extraction of endocrine-disrupting chemicals

EDCs are a new generation of environmental pollutants which causes an antagonistic effect to the endocrinal, reproductive, cardiological, and nervous systems.[77,78] A wide range of substances (both natural and man-made), such as polychlorinated

biphenyls (PCBs), dichlorodiphenyltrichloroethane (DDT), phthalates and phenols (mainly bisphenol A (BPA)), bisphenol AF (BPAF), 4-*n*-nonylphenol, 4-*n*-octylphenol are reported to cause endocrine disruption. Most of these substances are broadly used as surfactants and plasticizers in the production of food packaging materials.[79]

In view of the attempts to extract EDCs, Zhao *et al.* recently designed core–shell structured MagCOFs microspheres (Fe₃O₄@COF) by the reaction of 1,3,5-tris(4-aminophenyl) benzene (TAPB) and terephthaldicarboxaldehyde (TPA) with Fe_3O_4 as shown in Fig. 2.[80] The fabricated Fe₃O₄@COF microspheres were deployed in the selective extraction of four endocrine-disrupting phenols (4-*n*-nonylphenol, 4-*n*-octylphenol, BPA and BPAF) from plastic-packaged food, drinks and environmental water systems using a combination of MSPE with HPLC. The presence of surface functional groups (–COOH, –C═N, –NH₂) in Fe₃O₄@COF forms π–π interactions and hydrogen bonds with the specific sites of target molecules, which make them conducive for MSPE to extract target molecule from various samples. The proposed extraction mechanism involves the formation of hydrogen bonds between amino groups as well as C═N groups present on the surface of Fe₃O₄@COF microspheres and the hydroxyl groups of endocrine-disrupting phenols. Moreover, due to the presence of amino groups on Fe₃O₄@COF, the polarity and hydrophilicity of the particles gets improved, resulting in additional enhancement in extraction proficiency. Additionally, because of the large $\log K_{ow}$ (it is a ratio value without a unit and defines solubility of substance in water) and pK_a values of endocrine-disrupting phenols, they have a great tendency to escape from the water phase to the surface of Fe₃O₄@COF. Finally, the efficacy further increases due to the presence of π interactions between aromatic rings of COF shells and aromatic rings of endocrine-disrupting phenols. Besides, the indicative mesoporous structure of Fe₃O₄@COF also plays a vital role in the adsorption process by providing large surface area with appropriate surface functionalities. The excellent extraction performance is also attributed to the hydrophobicity of the material and the ionization of endocrine-disrupting phenols. Also, the other factors that ascribed to high adsorption performance of MagCOFs are hydrogen bonding, superparamagnetism, electrostatic interactions and ion-exchange. Besides, the coordination reaction

between composite materials and pollutants is also a key parameter. The method earned excellent linearity ($R \geq 0.995$) within the concentration range of 0.05–1000 ng mL⁻¹. The limit of detection (LOD) and limit of quantification (LOQ) were in the range of 0.08 ng mL⁻¹ to 0.21 ng mL⁻¹ (S/N = 3) and 0.39 ng mL⁻¹ to 0.85 ng mL⁻¹ (S/N = 10), respectively. Besides, the magnetic adsorbent showed high saturation magnetization (62.5 emu g⁻¹) and can be used for 20 runs without any loss in its adsorption capacity. The experimental data revealed that MagCOFs possess great potential as MSPE adsorbent for extracting various other pollutants from food. Hence, after the adsorption of pollutants using MagCOFs, the external magnet was used to assist their separation from aqueous media *i.e.*, if external magnet was removed, the MagCOF composites were dispersed again within a few seconds.

Likewise, Li and co-workers designed sensitive and efficient core–shell MagCOFs (NiFe₂O₄@COFs) *via* facile room temperature ultrasonic approach and the resulting magnetic nanocomposites were utilized for effervescent reaction-enhanced microextraction of endocrine disruptors in liquid matrices (Fig. 3).[81] The equilibrium adsorption capacity of six EDCs on magnetic adsorbent were found to be between 38.3 and 88.1 mg g⁻¹ which were primarily attributed to π–π interaction between analytes and MagCOFs. Moreover, NiFe₂O₄@COFs showed M_s value of 17.1 emu g⁻¹. The magnetic nanocomposites effervescent reaction-enhanced microextraction (MNER-EM-HPLC-FLD) method had good linearity in the range of 0.1–0.5–200 μg L⁻¹, high precision (relative standard deviations (RSDs) of 3.11–5.73%), good recoveries (83.4–106.2%) with lower LOD (0.019–0.096 μg L⁻¹) and R^2 (0.8952). Additionally, NiFe₂O₄@COFs could be reused for at least six cycles.

BPA is an another EDC which has been widely used to produce epoxy resins and polycarbonate plastics.[82,83] It is a pervasive contaminant which can interfere with endocrine systems of humans, wildlife and environmental health. In addition, it has been reported to induce a decrease in daily sperm count and fertility.[84] Thus, the removal of BPA and BPAF through selective and efficient adsorption has gained
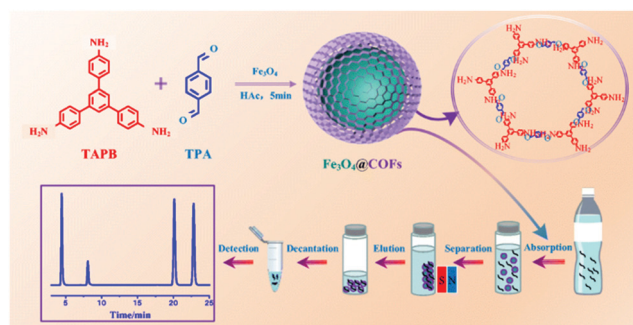

Fig. 2 Synthesis of Fe₃O₄@COF and extraction of EDCs. Reproduced with permission from ref. 80. Copyright 2019 Springer Nature Publishing AG.

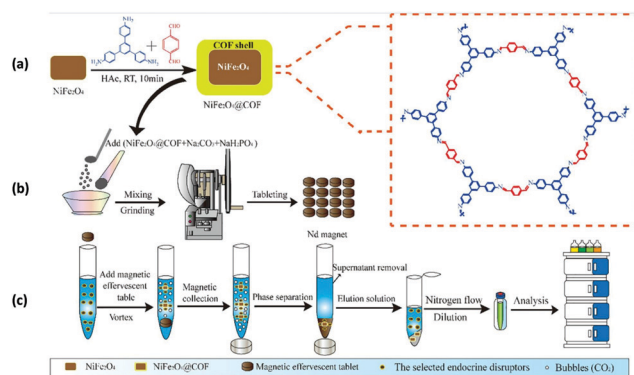**Fig. 3** Schematic diagram of the MNER-EM/HPLC-FLD method. (a) Synthesis of NiFe₂O₄@COF MNCs, (b) preparation of the magnetic effervescent tablets and (c) pre-concentration measurements and analytical procedures of EDCs by the MNER-EM/HPLC-FLD method. Reproduced with permission from ref. 81. Copyright 2020 Elsevier B.V.
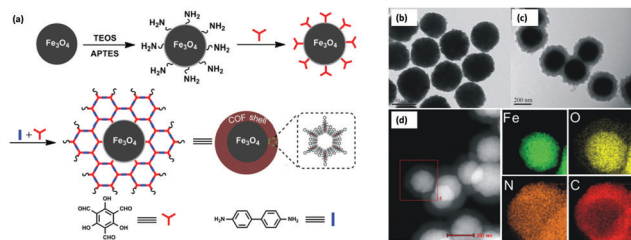
Fig. 4 (a)Monomer-mediated *in situ* strategy for synthesis of core–shell structured Fe_3O_4@TpBd nanospheres, TEM images of (b) Fe_3O_4, (c) Fe_3O_4@ TpBD and (d) HAADF-STEM image and EDX elemental mapping of Fe_3O_4@TpBD. Reproduced with permission from ref. 67. Copyright 2017 Royal Society of Chemistry.

tremendous attention in recent years. Though numerous adsorption methods have been developed so far, nearly all of them are associated with some drawbacks such as complicated synthetic procedure of the materials, prolonged time period, lower adsorption capacity of the material, slower adsorption kinetics, and many more. In this respect, considering the rising interest in the development of MagCOFs, Yan *et al.* designed monomer mediated *in situ* growth strategy for the controllable synthesis of core–shell structured MagCOF nanospheres, Fe_3O_4@TpBd, for the efficient adsorption and removal of EDCs, BPAF and BPA from aqueous solution (Fig. 4a).[67]

The Fe_3O_4@TpBd was designed in a very systematic manner: Fe_3O_4 NPs were initially synthesized *via* a solvothermal method, afterwards –NH_2 groups were introduced on the surface of magnetic core to produce amino functionalized nanospheres (Fe_3O_4–NH_2) to avoid aggregation of MNPs as well as to incorporate polar surface functionalities. Furthermore, a monomer of TpBd, 1,3,5-triformylphloroglucinol (Tp), was grafted over Fe_3O_4–NH_2 *via* Schiff base condensation reaction for *in situ* growth of COF shell. To acquire uniform crystalline growth of COF shell, pre-grafting of monomer played a crucial role. The pre-grafting of monomer Tp acts as a bridge between magnetic core and COF shell to achieve better interaction and helps to nucleate the centers for uniform COF growth. Further, another monomer benzidine (Bd) was grafted over uniform core–shell through imine bond formation. Additionally, TEM, HAADF-STEM and EDX elemental mapping data confirmed a typical core–shell structure of Fe_3O_4@TpBd nanospheres (with TpBd thickness being 15–65 nm) (Fig. 4b–d). Moreover, the choice of solvent and concentration of monomers acts as key factors to control the thickness and crystallinity of COF shells.

The as-synthesized Fe_3O_4@TpBd was then explored for adsorption of BPA and BPAF and displayed higher adsorption capacity with faster adsorption kinetics followed by facile magnetic separation. The adsorption equilibrium was achieved within 5 min for BPA and BPAF. The adsorption isotherms of BPA and BPAF on Fe_3O_4@TpBD illustrate a typical Langmuir adsorption with the maximum adsorption capacities of 160.6 and 236.7 mg g^{-1}, respectively. Fe_3O_4@TpBd showed excellent reusability up to five runs, which rendered them as novel adsorbent for aqueous solution adsorption.

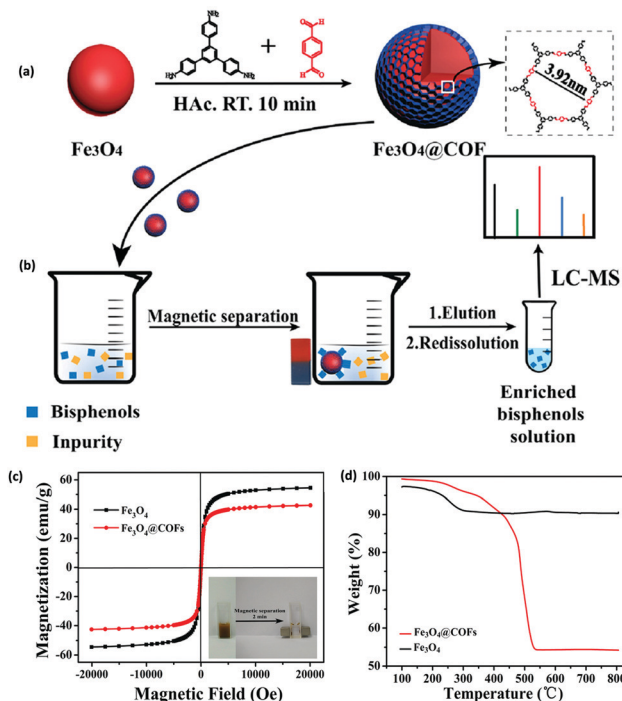**Fig. 5** (a) Preparation of the Fe_3O_4@COF nanocomposites and (b) MSPE process for extraction of BPs in human serum sample, (c) VSM curves of Fe_3O_4 and Fe_3O_4@COFs and (d) TGA curve of Fe_3O_4 and Fe_3O_4@COFs. Reproduced with permission from ref. 70. Copyright 2018 Elsevier B.V.

In a similar fashion, extraction of BPs from human serum sample using MNPs immobilized COF, Fe_3O_4@COF, was studied by Lin and co-workers (Fig. 5).[70] The core–shell structured magnetic adsorbent was fabricated by immobilizing two building units, TAPB and TPA on the surface of MNPs (of size 250 nm) *via* Schiff base condensation reaction at room temperature. Further, the adsorption efficiency of Fe_3O_4@COF (with COF thickness being 25 nm) was investigated by evaluating their adsorption isotherms and adsorption kinetics. Further, to determine the magnetic properties of bare Fe_3O_4 and Fe_3O_4@COF, VSM was used. From Fig. 5c, it can be noted that M_s value decreases from Fe_3O_4 (54.5 emu g^{-1}) to Fe_3O_4@ COF (42.7 emu g^{-1}) which can be attributed to grafting of COF shell over Fe_3O_4. The inset of Fig. 5c display that Fe_3O_4@COF nanocomposite was dispersed in aqueous solution and separated with the aid of external magnet within 2 minutes. Besides, thermogravimetric analysis (TGA) of Fe_3O_4 and Fe_3O_4@COF showed weight loss of 6% and 48% respectively, which implies high yield of COF shells over MNPs in the temperature range of 100–350 °C. Fe_3O_4@ COF showed excellent thermal stability under 300 °C (Fig. 5d). Moreover, due to high porosity, high thermal and chemical stability and large specific surface area (181.36 m^2 g^{-1}) of magnetic adsorbent, equilibrium was attained very quickly, indicating fast adsorption kinetics and size selectivity. The high adsorption of BPs was achieved due to van der Waals forces and strong π–π interactions between COF shells and benzene rings of BPs.

The developed protocol possessed good linearity in the range of 0.1–50 µg L^{-1} with $R^2 \geq 0.9982$. Besides, LODs were

found to be between 1.0 to 78.1 ng L^{-1} with high enrichment factor (56–95-fold). The RSDs were less than 3.4% for inter-day and 6.9% for intra-day. Moreover, the authors assessed the performance of Fe$_3$O$_4$@COF in real samples and satisfactory results were obtained with recoveries ranging from 93.0–107.8%. The additional advantage of the developed adsorbent was its ability to be recycled and reused for twelve adsorption–desorption cycles.

3.2 Extraction of persistent organic pollutants

Over several decades, the exposure of humans and wildlife to environmental contaminants has been a global concern. PCBs are a class of POPs that exert various detrimental effects on humans and wildlife, such as neurotoxicity, immunotoxicity, reproductive toxicity and carcinogenicity.[85,86] PCBs can be metabolized as hydroxylated PCBs (–OH PCBs) in higher organisms including humans and animals via cytochrome P450 enzyme-mediated oxidation mechanism. The –OH PCBs are produced in the environment by the oxidation of PCBs through both metabolic transformations (in living organisms) and abiotic reactions (with hydroxyl radicals). At present, –OH PCBs are being detected in animal tissue sample, water, sediment and even in human blood (which often leads to endocrine toxicity).[87] Hence, –OH PCBs have raised serious environmental concerns due to their toxic effects and therefore, it is quintessential to develop an efficient method for the extraction of –OH PCBs.

On a similar note, an aptamer functionalized magnetic core–shell structured conjugated organic framework (Fe$_3$O$_4$@COFs-Apt) has been developed for the selective extraction of trace –OH PCBs from human serum sample (Fig. 6a and b).[36] An aptamer is a single strand DNA/RNA molecule, having high binding affinity towards target molecule through van der Waals, electron–acceptor–donor and hydrogen-bonding interactions. For the synthesis of Fe$_3$O$_4$@COFs-Apt, firstly, MNPs were synthesized by two conventional methods, i.e., co-precipitation and solvothermal method. To improve chemical stability and to avoid agglomeration, bare MNPs were coated with silica using tetraethyl orthosilicate (TEOS). Relatively inexpensive and simple silica coating not only minimizes the aggregation but also provides many potential benefits such as chemical inertness, high binding strength with iron-oxide core,

robustness, possibility for further functionalization, etc.[88–95] Further, amino groups were introduced on the surface of Fe$_3$O$_4$@SiO$_2$ to obtain amino-modified Fe$_3$O$_4$@SiO$_2$@NH$_2$. Afterwards, the monomers, p-phenylenediamine (PPD) and trimesoyl chloride (TMC) were added to obtain carboxylic acid rich MagCOFs (Fe$_3$O$_4$@COFs-COOH). Thus, to enhance the extraction efficiency, aptamers were immobilized on the surface of MagCOFs (Fe$_3$O$_4$@COFs-Apt) via covalent linkage between surface carboxylic groups and the amino groups of the aptamers. Fe$_3$O$_4$ with average size of 150 nm were obtained by solvothermal method, denoted as Fe$_3$O$_4$@COFs-Apt-150 and Fe$_3$O$_4$ with an average size of 15 nm were obtained by co-precipitation method and denoted as Fe$_3$O$_4$@COFs-Apt-15.

The N$_2$ adsorption–desorption isotherms revealed that Fe$_3$O$_4$@COFs-Apt-15 had higher surface area and hence considered as a better adsorbent material. Subsequently, Fe$_3$O$_4$@COFs-Apt-15 was deployed for the extraction of hydroxy-2′,3′,4′,5,5′-pentachlorobiphenyl (2-OH-CB 124). To check the selectivity of Fe$_3$O$_4$@COFs-Apt-15 for 2-OH-CB 124, three other compounds such as 4′-hydroxy-2,3,3′,5,6-pentachlorobiphenyl (4′-OH-CB 112), 4-hydroxy-2,3,4,5-tetrachlorobiphenyl (4′-OH-CB 61) and 4′-hydroxy-2,4,6-trichlorobiphenyl (4′-OH-CB 30) were selected to conduct unspecific tests. The results unveiled that Fe$_3$O$_4$@COFs-Apt-15 displayed highest recovery of >90% for 2-OH-CB 124, indicating the superior extraction efficiency of 2-OH-CB 124 (Fig. 6c). The adsorption ability for above four compounds was also investigated with Fe$_3$O$_4$-15 and Fe$_3$O$_4$@COFs-COOH-15 only to obtain satisfactory recoveries with Fe$_3$O$_4$@COFs-Apt-15. The presence of π–π stacking interaction, high surface area and hydrophilic property (raised from carboxylic group) increased the adsorption capacity of Fe$_3$O$_4$@COFs-Apt-COOH-15. Meanwhile, Fig. 6c depicts that in comparison with Fe$_3$O$_4$@COFs-Apt-15, Fe$_3$O$_4$@COFs-COOH-15 could not provide satisfactory selectivity for 2-OH-CB 124 (recoveries <25%), which indicates that aptamer played a substantial role towards selectivity of 2-OH-CB 124 due to their highly specific binding affinity. Under optimized conditions, Fe$_3$O$_4$@COFs-Apt-15 showed great potential in determination of 2-OH-CB 124 from human serum samples with recoveries in the range of 87.7–101.5%. The MSPE-LC/MS coupled method exhibited good linearity in the range of 0.01–40 ng mL^{-1} with excellent R^2 value of 0.9973. The LOD was low (2.1 pg mL^{-1}) with a satisfactory LOQ (6.7 pg mL^{-1}). Besides providing easy magnetic recoverability, the adsorbent could be recycled for ten extraction cycles.

Poly aromatic hydrocarbons (PAHs) are a type of POPs that have long been considered as hazardous for both human and environment. They mainly originate from anthropogenic activities such as pyrolysis of organic materials such as oil, coal, wood and petroleum gas. Due to highly mutagenic, carcinogenic and teratogenic potential of PAHs, they are one of the greatest environmental and economic threats to our society.[96] In this regard, Cai et al. fabricated a gypsophila bouquet-shaped MagCOF, TpPa-1, by grafting COF over the surface-modified MNPs, for enhanced extraction of PAHs from environmental samples (Fig. 7).[71] The novel TpPa-1 was synthesized
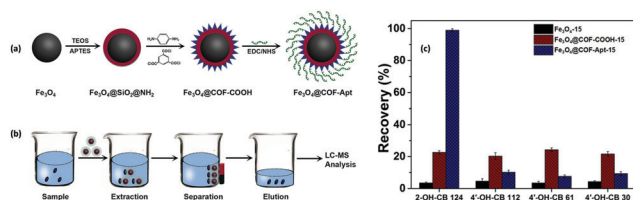

Fig. 6 (a) Synthetic illustration for the synthesis of Fe$_3$O$_4$@COFs-Apt, (b) typical process for selective extraction of OH-PCBs with Fe$_3$O$_4$@COFs-Apt and (c) comparison of extraction efficiency of 2-OH-CB 124, 4′-OH-CB 112, 4′-OH-CB 61 and 4′-OH-CB 30 with Fe$_3$O$_4$-15, Fe$_3$O$_4$@COFs-COOH-15 and Fe$_3$O$_4$@COFs-Apt-15. Reproduced with permission from ref. 36. Copyright 2018 John Wiley & Sons.
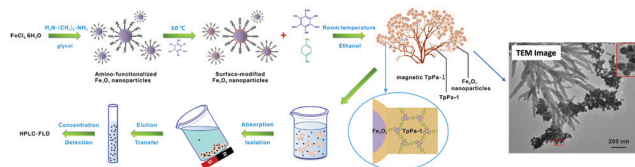
Fig. 7 Synthesis and application of the bouquet-like magnetic TpPa-1 sorbent. Reproduced with permission from ref. 71. Copyright 2017 American Chemical Society.

Fig. 8 (a) Synthesis of COF-LZU1@PEI@Fe$_3$O$_4$ and TEM images of (b) PEI@Fe$_3$O$_4$ and (c) COF-LZU1@PEI@Fe$_3$O$_4$. Reproduced with permission from ref. 97. Copyright 2021 Springer Nature Publishing AG.

by facile room temperature solution-phase approach and utilized the advantageous properties of both MNPs and COF. Initially, surface-modified Fe$_3$O$_4$ nanoparticles (of size 30 nm) were synthesized by pre-grafting of monomer Tp onto amino functionalized Fe$_3$O$_4$ nanoparticles. This process helped in acquiring uniform COF shell by generating COF centers *via* Schiff base reaction. Further, another monomer, phenylenediamine (Pa-1) was added under mechanical agitation to obtain magnetic TpPa-1. The TEM image in Fig. 7 clearly depicts the gypsophila bouquet-shaped structures of TpPa-1. Magnetic TpPa-1 possessed superparamagnetism (40.1 emu g^{-1}) as well as large surface area and high porosity.

The as-synthesized magnetic TpPa-1 was further explored for the extraction of PAHs. Initially, magnetic TpPa-1 was directly dispersed into filtered water sample spiked with PAHs and further subjected to ultrasonication followed by additional shaking for 20 min. After extraction of analytes, the sorbent was gathered using external magnet and the supernatant was subjected to HPLC-FLD system for further detection. Moreover, it was anticipated that TpPa-1 might extract organic targets containing benzene ring, amino or hydroxyl groups due to the presence of high percentage of oxygen and nitrogen atoms as well as large π–π framework. The fabricated nanocomposite exhibited an excellent linear range of 2.0–200.0 ng L^{-1} with a good R^2 of 0.9993, with LOD ranging from 0.24–1.01 ng L^{-1}. Furthermore, the material possessed good reusability and could be applied in real sample analysis including lake water, tap water and river water with percentage recoveries of PAHs over 73–110% with a lower RSD value (2–8%). Inspired by encouraging extraction efficiencies of magnetic TpPa-1 towards PAHs, it is expected that the bouquet shaped MagCOF could also have strong affinity towards other chemicals. Besides, magnetic TpPa-1 can also be utilized in wider applications by post-synthetic modification approach.

Similarly, a new and promising class of COF has been synthesized by Chen and group for PAHs extraction.[97] They synthesized COF-LZU1@PEI@Fe$_3$O$_4$ *via* covalent immobilization of COF-LZU1 (imine-based COF, prepared by Schiff base reaction of 1,3,5 triformyl benzene (Tb) and 1,4 diaminobenzene) on PEI-functionalized MNPs (Fig. 8a). Firstly, MNPs were coated with polyethyleneimine (PEI) by electrostatic interactions (PEI@Fe$_3$O$_4$). Thereafter, several active amino groups present on PEI enhanced the covalent bonding between the PEI layer and COF-LZU1, due to which COF shells were grown on the surface of MNPs through Schiff base reaction. The designed method was further applied for the extraction of six
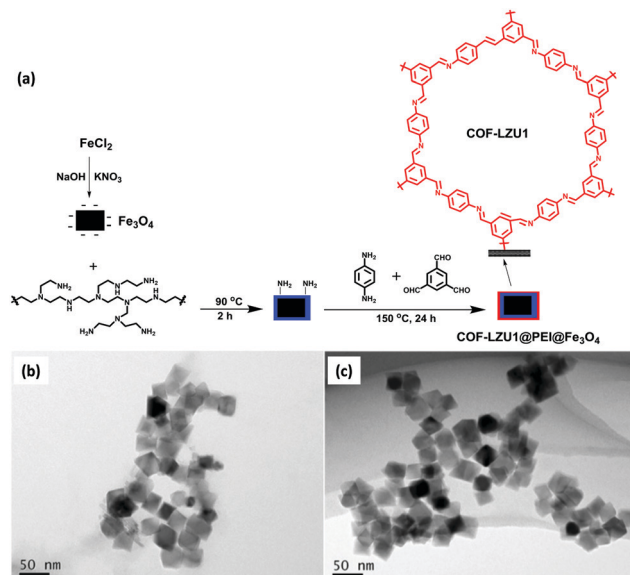
PAHs from environmental and real samples by MSPE coupled with HPLC. The concentration level of PAHs in an environmental sample is quite low to determine directly by analytical instrument. So, their pretreatment using MSPE was necessary prior to HPLC. COF-LZU1@PEI@Fe$_3$O$_4$ exhibited high surface area, excellent thermal stability and high porosity, which increased the loading capacity of the adsorbent. As discussed earlier, the presence of aromatic rings and imine groups in COF led to strong π–π stacking and hydrophobic interaction with analytes. These characteristics made them an attractive material for solid phase extraction of PAHs. The TEM images showed that PEI@Fe$_3$O$_4$ and COF-LZU1@PEI@Fe$_3$O$_4$ display beautiful cubic morphology with mean diameter of 40 nm (Fig. 8b and c). Also, it can be noted that surface of PEI@Fe$_3$O$_4$ was smooth and after modification with COF-LZU1, a rough and thin polymer layer was observed (due to porous structure of COF-LZU1) which confirms immobilization of COF-LZU1 over PEI@Fe$_3$O$_4$.

To optimize the extraction efficiency, various parameters were investigated, such as the effect of temperature, type of solvent, pH of the sample solution, extraction time and sampling volume. Due to the presence of highly hydrophobic aromatic rings in PAHs, the addition of small amount of acetonitrile facilitates their solubility in aqueous sample solution. Further, it was observed that when acetonitrile content increased from 0.5% to 1%, PAH extraction efficiency increases while it decreases when acetonitrile content increases from 2% to 10%. Hence, results stated that a certain amount of acetonitrile do facilitates the solubility in sample solution. Best extraction was achieved when 1% acetonitrile was used as a solvent. Further, sample pH was investigated from 4.0 to 9.0. It can be noted that as pH varies from 4.0 to 9.0, extraction efficiency of PAH increases. This is because H$^+$ can affect the

interaction between PAH and adsorbent. Then, with decrease in pH value, the –NH_2 groups present on COF-LZU1 would change to NH_3^+ and this would decrease the π-electron cloud density and weak π–π stacking interaction by its electron-withdrawing inductive effect. Thus, for better extraction efficiency 9.0 was selected as sample pH value. The extraction time was 30 min with a sample volume of 20 mL. Under optimized conditions, the extraction performance of COF-LZU1@PEI@Fe_3O_4 was evaluated. The results showed that COF-LZU1@PEI@Fe_3O_4 displayed significant extraction efficiency. The combination of MSPE and HPLC methods showed good linear range with R^2 higher than 0.9989. The LOQ was 0.5–50 pg mL^{-1}. Besides, the adsorbent could be reused for up to six cycles. The above research expands the scope of MagCOFs as adsorbents for extraction of various other pollutants.

3.3 Extraction of triazole fungicides

Triazole fungicides (TFs) are the systematic broad-spectrum fungicides which usually contain hydroxyl/ketone groups, unique 1,2,4-triazole ring and substituted phenyl ring in the main chain.[98] TFs are widely used in agricultural production mainly to protect crops from various fungal diseases. Also, TFs have been used in leather, textile industries, wood preservatives, paints and antifouling agents and considered as the largest fungicide category by the global market value.[99] However, they can enter into multiple environmental media through surface run offs and contaminate agricultural products, surface water, human urine, soils and hair samples. Exposure to TFs causes adverse health effects such as liver carcinogenicity, reproductive and development toxicities, hepatic toxicities and endocrine disruption.[99] Hence, their efficient detection and effective removal are highly imperative.

In this context, Hu et al. fabricated magnetic porous organic polymers (MOPs) via simple azo reaction under mild reaction conditions between monomer, TAPB and 1,3,5-trihydroxy-benzene using Fe_3O_4@SiO_2 as the magnetic core (Fig. 9a).[37] The as-synthesized MOPs (having 5 nm thick polymer layer) have been utilized as an adsorbent for the extraction of five target TFs (triazolone, penconazole, hexaconazole, diniconazole and tebuconazole) from vegetables by MSPE. For the desorption of TFs, organic solvents with different polarity such as ethyl acetate, acetonitrile, mixed solvents (acetone : ethyl acetate (1 : 1/v/v)) and acetone were used but best results were obtained when ethyl acetate was used as a desorption solvent. The MSPE-GC-FID showed good linearity in the range of (0.5–200 μg L^{-1} with R^2 > 0.9991–0.9998). The LOD for five target TFs was found to be in the range of 0.12–0.19 μg L^{-1} according to the three-fold signal-to-noise ratio. Moreover, lower RSDs value (2.6–6.8%), efficient extraction efficiency (84.5–90.3%) and reusability up to five runs demonstrated its excellent performance. The developed MSPE-GC-FID was facile, rapid, selective and sensitive and proved its incredible potential towards extraction of TFs.

3.4 Extraction of triclosan and triclocarban

Over the past few years, pharmaceutical and personal care products (PPCPs) have emerged as one of the most hazardous
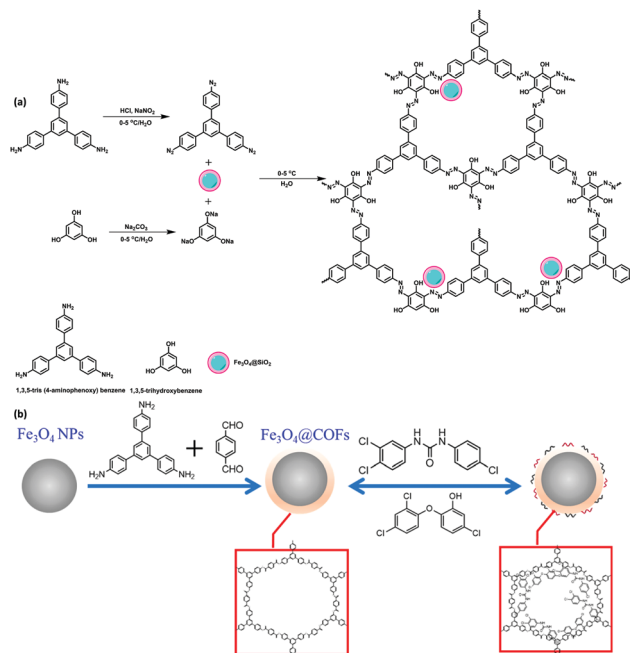
Fig. 9 (a) Preparation of MOPs, and (b) Synthesis of Fe_3O_4@COFs. Reproduced with permission from ref. 100. Copyright 2019 American Chemical Society.

groups of environmental contaminants.[101] PPCPs include a diverse range of chemical substances which cause potential adverse effects to humans, wildlife and aquatic organisms. Hence, it is essential to control the pollution level originating from PPCPs. Among the variety of PPCPs, triclosan (TCS) and triclocarban (TCC) are two chlorinated antimicrobial additives which have been broadly used in detergents for sanitation.[102] However, their incomplete removal often leads to several health and environmental problems such as endocrine-disrupting effect, bioaccumulation in snails and algae, development of microbial resistance and many more.[103,104] Due to its rising concentration in environment and the abovementioned health effects, there is a need for the development of reliable treatment methods to remove these contaminants.

On this note, Cai et al. fabricated Fe_3O_4 (MNPs) supported core–shell structured MagCOF, Fe_3O_4@COF, for the efficient extraction and rapid removal of TCC and TCS from water and serum samples (Fig. 9b).[100] To fabricate Fe_3O_4@COF, MNPs (of size 165 nm) were first synthesized via solvothermal method. Further, COF shell was introduced on the surface of bare Fe_3O_4 by Schiff base condensation reaction of monomer TAPB and TPA in DMSO at room temperature. Additionally, the adsorption performance of Fe_3O_4@COF was investigated by Langmuir and Freundlich adsorption isotherms. The Langmuir model was more appropriate in the high concentration region while Freundlich isotherm was more appropriate in the low concentration region. Also, Langmuir and Freundlich isotherms displayed monolayer adsorption at high concentration range and multilayer adsorption at low concentration, respectively. The monolayer adsorption took place due to strong π–π stacking interactions between the interface of TCS, TCC and Fe_3O_4@COF

while multilayer adsorption was due to van der Waals forces, π–π interactions among phenyl rings and space embedding interaction. Moreover, the adsorption kinetics followed a pseudo-second-order kinetic model.

The quantitative analysis of TCC and TCS was determined using UHPLC-MS/MS. The results stated good linearity in the range of 0.05–25 ng mL^{-1} for TCC and 0.1–50 ng mL^{-1} for TCS with R^2 greater than 0.9976. The LODs for TCC and TCS were 0.005 and 0.02 ng mL^{-1}, respectively. The method was further applied to remove TCC and TCS from healthy fetal bovine serum samples and showed excellent recoveries in the range of 92.9–109.5% and 82.3–95.4% for TCC and TCS, respectively. Moreover, the adsorbent was reused for ten adsorption–desorption cycles with similar extraction efficiency. With the combination of marvellous characteristics of COF and magnificent properties of Fe_3O_4, Fe_3O_4@COF served as a potential candidate for the treatment of environmental and biological samples.

3.5 Diclofenac extraction

Diclofenac sodium is a widely used non-steroidal anti-inflammatory drug for treating several types of inflammatory disorders.[105] Since past few years, it has gained increasing global concern due to its frequent detection in surface, ground and aquatic environment and even in drinking water. It has also found to be responsible for causing aquatic ecotoxicity and severe renal failure because of its extremely low biodegradability.[106] Thus, there is need for the development of cost-effective, efficient and reliable technique for the removal of diclofenac sodium from adulterated water bodies.

Continuing the utility of MagCOFs, Shuai et al. developed a MagCOF via salt-mediated crystallization strategy under solvent free environment for the removal of diclofenac sodium from water. The fabrication procedure involved the grafting of Tp and p-phenylenediamine (PDA) on amino-functionalized MNPs using p-toluenesulfonic acid as catalyst (Fig. 10).[107] Fig. 10b and c shows narrow size distribution and uniform spherical morphology of Fe_3O_4 nanospheres with mean diameter of 10–15 nm. Also, the magnetite nanoparticles are tightly shelled by SiO_2. Besides, MagCOF-2 shows that MNP-NH$_2$ is well encapsulated in COF framework. Adsorption isotherms displayed a Freundlich isotherm which was well fitted in case of adsorption of diclofenac sodium on MagCOF-2 with a high R^2 value ($\sim$0.99) of the curve and a maximum adsorption capacity of 565 mg g^{-1}. The adsorption equilibria were achieved within 20 min indicating the supremacy of MagCOF-2 towards diclofenac sodium removal. The value of Freundlich constant ($n > 1$) revealed that the adsorption of diclofenac sodium was favourable. Moreover, the experimental data reflected that the effective adsorption is caused by π–π stacking, hydrogen bonding and electrostatic interactions. Additionally, with excellent magnetization and high specific surface area, the as-synthesized magnetic adsorbent could be reused for five cycles without any significant loss of its adsorption capacity. The applicability of MagCOF-2 was also assessed in actual water samples. Interestingly, the results ascribed superior potential of MagCOF-2 for diclofenac sodium removal.
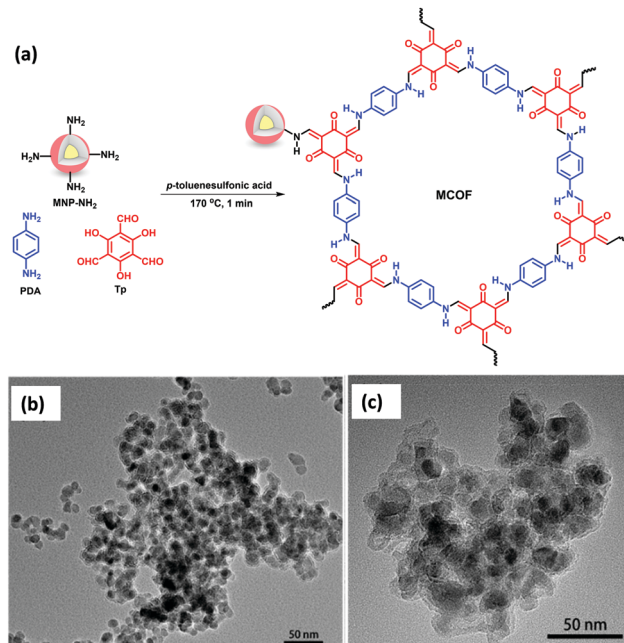

Fig. 10 (a) Synthesis of MagCOF-2 via a solvent free, salt-mediated crystallization strategy, TEM images of (b) MNP-NH$_2$ and (c) MagCOF-2. Reproduced with permission from ref. 107. Copyright 2019 American Chemical Society.

Similar to the previously discussed MNPs grafted COF, Wang et al. designed few other MagCOFs by facile impregnation method for the removal of diclofenac and sulfamethazine (SMT). For the synthesis, firstly, TPB-DMTP-COFs were synthesized using the reaction between dimethoxyterephthaldehyde (DMTP) and TAPB monomers. Secondly, the as-synthesized TPB-DMTP-COF was reacted with a solution containing Fe^{2+} and Fe^{3+} followed by membrane separation. Finally, separated solids were immersed in ammonia solution to yield Fe_3O_4 in COF structure, (Fig. 11).[108] The adsorption activity of the MagCOF was evaluated by adsorption kinetics and isotherms. Adsorption kinetics revealed that equilibria were achieved within 50 min for the removal of diclofenac and 80 min for
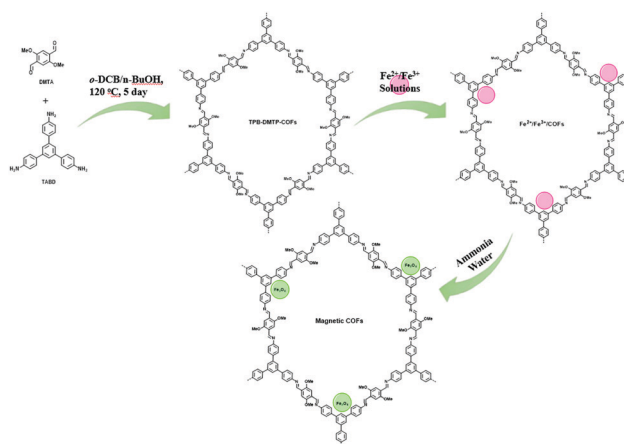

Fig. 11 Synthetic steps of MagCOFs.

SMT removal with a maximum adsorption capacity of 40.4 mg g^{-1} and 55.24 mg g^{-1}, respectively. From the experimental data it was noted that pseudo-first-order model was better in diclofenac adsorption while SMT adsorption was well described by pseudo-second-order kinetic model with $R^2 > 0.99$ in both cases. In addition, the adsorption process of diclofenac and SMT was well defined by Sips isotherm model. By Sips model, the maximum adsorption capacity of diclofenac and SMT was found to be 109 mg g^{-1} and 113.2 mg g^{-1}, respectively. Furthermore, the adsorption mechanism was studied by density functional theory (DFT) which revealed that the adsorption took place by C–H···π interaction. The adsorption energies were calculated to be −47.8 kJ mol^{-1} and −63.2 kJ mol^{-1} for SMT and diclofenac, respectively. When the efficacy of the magnetic adsorbent was compared with previously reported adsorbents, MagCOF showed higher adsorption capacity.

3.6 Paclitaxel extraction

Paclitaxel is known as a key component in the treatment of numerous solid tumors including breast, lung and refractory ovarian.[109] Their therapeutic effect is mediated on the polymerization of tubulin, thereby causing suppression/cell death of microtubule dynamics during cell division without changing microtubule mass.[110] Paclitaxel was approved as an anti-cancer drug by U.S. FDA in 1992.[111] The examination of paclitaxel in urine, plasma and other bio-fluids is essential for pharmacotoxicology, pharmacodynamics and pharmacokinetic evaluation. However, due to the low levels of paclitaxel in bio-fluids, their pretreatment is highly demanded prior to instrumental analysis. In this regard, Chen *et al.* developed COF-1 modified MNPs (Mag-COF-1) for the selective extraction of paclitaxel from rat plasma samples by combining the merits of MSPE with HPLC (Fig. 12a).[41] Mag-COF-1 was fabricated by the bioinspired polydopamine method through immobilization of layered hexagonal COF-1 framework (constructed *via* self-molecular dehydration reaction of BDBA), on the surface of MNPs through catechol groups. Polydopamine played a significant role in the immobilization process due to the presence of catechol groups. Further, Mag-COF-1 was utilized in adsorption of paclitaxel. Moreover, selective extraction of paclitaxel was attributed to the hydrophobic interaction, π–π interaction

and host–guest interaction among phenyl rings present in Mag-COF-1 and the functional moieties present in paclitaxel. Additionally, TEM images of M-PEI showed uniform cube like morphology and a smooth layer was introduced over M-PEI (M-PEI; 40 nm) in case of Mag-COF-1 (Fig. 12b and c). The developed MSPE-HPLC method offered outstanding linearity in the range of 0.1–200 ng mL^{-1} and a lower LOD (0.02 ng mL^{-1}). The chromatograms of plasma samples show that after extraction paclitaxel was efficiently enriched and showed good clean-up capacity (Fig. 12d). Paclitaxel content in medicated plasma samples was calculated to be 3.28 μg mL^{-1}. The RSD value was less than 2.3% confirming excellent recoveries in the range of 99.4–103.7%. M-COF-1 was easy to recycle and which could be reused up to six runs under the same conditions. Good linearity, high accuracy and good selectivity showed that the proposed method was efficient and sensitive for the extraction of paclitaxel.

3.7 Sulfonamides extraction

Sulfonamides (SAs) represent a most important class of synthetic anti-microbials, which have been widely practiced for the treatment of bacterial infections.[112] Also, world widely they have been utilized to treat both human and veterinary diseases. Owing to their high efficacy, low-cost, and broad-spectrum anti-microbial activities, they have been used in aquaculture and livestock. However, the uncontrolled use of SAs and their continual discharge to aquatic environment lead to emiction, resistant bacteria in human body, hemopoiesis and carcinogenicity.[113] Additionally, water-borne SAs can enter the food chain and cause severe allergic reactions to human. Hence, it is important to develop a highly sensitive and efficient method to detect SAs in environmental and food samples.

In view of this, Zhang *et al.* developed porphyrin-based MagCOF (Fe$_3$O$_4$@COF) for the extraction and analysis of six SAs (sulfamerazine (SMR), sulfadiazine (SDZ), sulfamethazine (SMZ), sulfamethoxazole (STZ), sulfamonomethoxine (SMX) and sulfadimethoxine (SDM)).[114] For the synthesis, firstly, amino-functionalized MNPs were formed *via* facile one-pot strategy. Further, COF shells were grown on the surface of amino-functionalized nanospheres using dehydration reaction between two organic ligands namely 4,4′-biphenyldicarboxaldehyde and TAP (Fig. 13a). The presence of amino groups on the surface of Fe$_3$O$_4$ nanospheres facilitated the *in situ* COF growth *via* Schiff base reaction. Moreover, the presence of nitrogen containing heterocyclic ring in porphyrin-based COF offers specific multiple-interactions *i.e.*, π–π interaction, hydrogen bonding, hydrophobic and electrostatic interactions with target analytes. Fig. 13b and c showed that the as-obtained Fe$_3$O$_4$@COF (10 ± 2 nm thickness) nanospheres were spherical in shape with average size of 100 ± 14 nm.

Thereafter, to check the superiority of the Fe$_3$O$_4$@COF nanospheres, the extraction of six SAs were evaluated systematically using MSPE coupled with HPLC. In the extraction process, initially, the target analyte SAs were pre-treated *via* sample pre-treatment technique (MSPE) and further subjected to quantitative analysis *via* HPLC. The chromatograms of six SAs with extraction, without extraction and by using Fe$_3$O$_4$
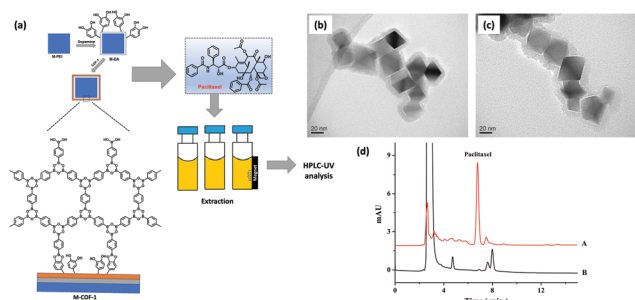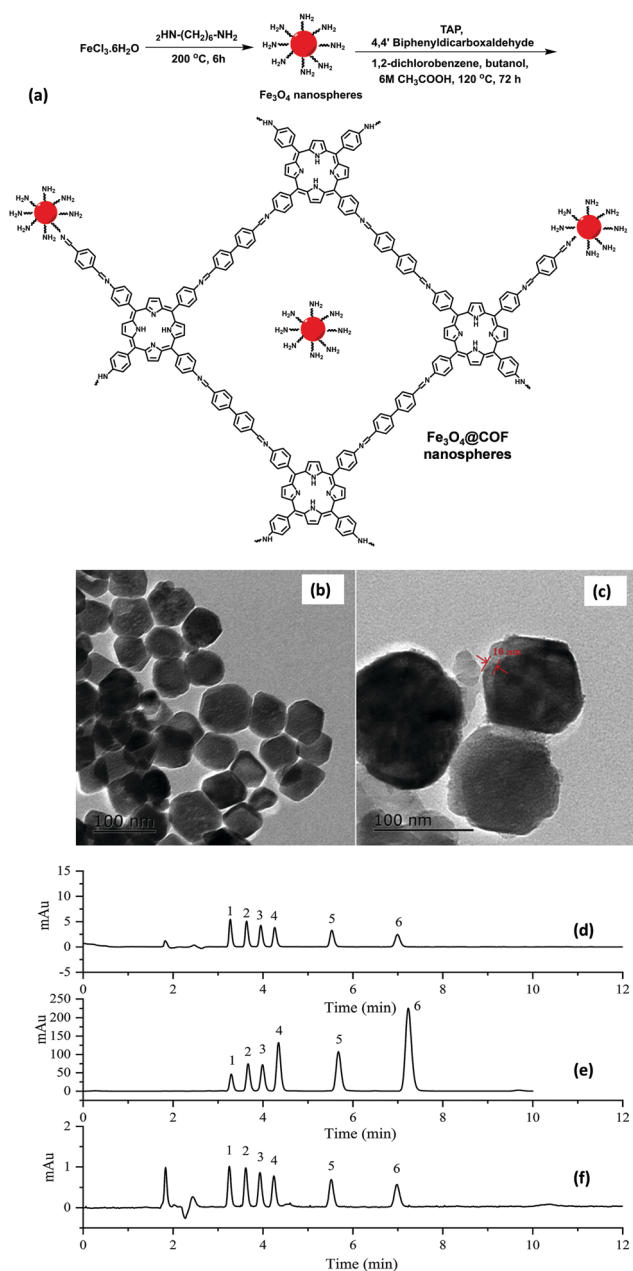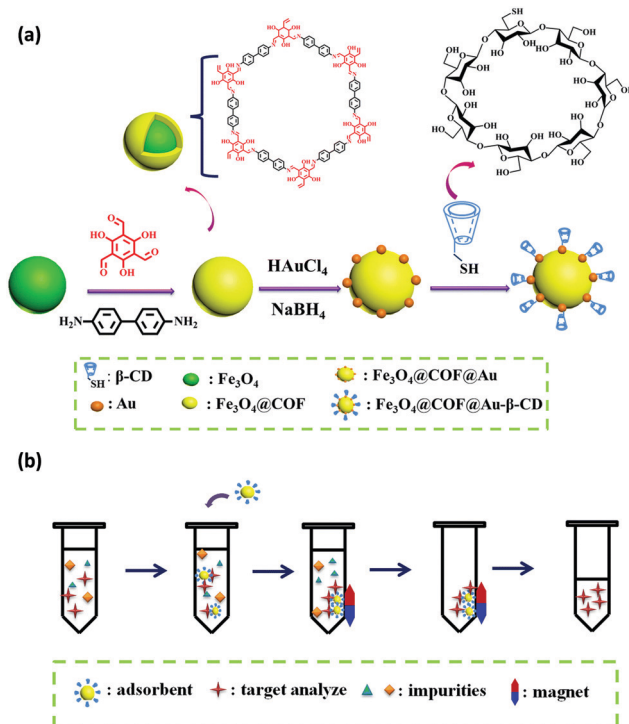

Fig. 12 (a) Synthesis of Mag-COF-1 and extraction of paclitaxel, TEM images of (b) M-PEI and (c) Mag-COF-1 and (d) chromatograms of rat plasma samples (A) with extraction and (B) without extraction. Reproduced with permission from ref. 41. Copyright 2016 Elsevier B.V.

Fig. 13 (a) Synthesis of Fe$_3$O$_4$@COFnanospheres, TEM images of (b) Fe$_3$O$_4$, (c) Fe$_3$O$_4$@COF, and chromatograms of six SAs standard solutions (d) before extraction, (e) after extraction by core–shell structured Fe$_3$O$_4$@COFs nanospheres and (f) after extraction on bare Fe$_3$O$_4$ nanospheres under optimum condition. Peak identity: 1, SDZ; 2, SMR; 3, SMZ; 4, SMX; 5, STZ; 6, SDM. Reproduced with permission from ref. 114. Copyright 2019 Elsevier B.V.

Fig. 14 (a) Schematic illustration for the synthesis for Fe$_3$O$_4$@COF@Au-β-CD and (b) the MSPE procedure for the determination of SAs in meat. Reproduced with permission from ref. 114 Copyright 2020 Springer Nature Publishing AG.

nanospheres are shown in Fig. 13d–f, which illustrates the high extraction efficiency of core–shell Fe$_3$O$_4$@COF nanospheres. The results revealed that out of the six SAs, SMX and SDM with methoxy groups substituted on pyrimidine ring displayed higher extraction efficiency instead of methyl substitution. The reason stated that the methoxy group could form conjugation which lowered the basicity of pyrimidine ring, thereby enhancing the electrostatic and π–π interaction with porphyrin ring than that of methyl substitution. From Fig. 13f, it is observed that in comparison to Fe$_3$O$_4$@COF, bare Fe$_3$O$_4$ showed much lower peak area of SAs extraction. This is due to multiple interactions between COF layer and SAs. Also, Fe$_3$O$_4$@COF showed strong adsorption affinity for SAs due to their high surface area and porosity, which also leads to enhancement of extraction efficiency. The method presented a wide linear range from 1 to 500 ng mL^{-1}. The LOD for six SAs were ranged from and 0.2–1 ng mL^{-1} with R^2 higher than 0.99. Further, the established method was applied in real samples including milk, pork, chicken, lake water and shrimp for the detection of SAs. The MSPE-HPLC method showed excellent recoveries (65.3–107.3%) in environmental water and food with RSD ≤ 6.7. Hence, specific surface area, high stability, good porosity and large π-conjugated system endowed Fe$_3$O$_4$@COF nanospheres as an excellent sorbent for the analysis of SAs.

Likewise, Zhou and co-workers fabricated thiolated-β-cyclodextrin-functionalized MagCOFs for the extraction of trace SAs from meat samples (Fig. 14).[115] The approach involved amino-modified MNPs as the support material. In this case, β-CD could form inclusion complexes via capturing targeted analytes into its cavity through host–guest relationship. It was prepared by direct solvothermal method by taking FeCl$_3$ as the iron source and ((3-aminopropyl)triethoxysilane) (APTES) as –NH$_2$ source (to facilitate the Schiff base reaction between COF monomers and magnetic core). After its formation, the monomers Tp and Bd were covalently grafted on the surface of

Fe_3O_4-NH_2 to form Fe_3O_4@COF. Further, Fe_3O_4@COF@Au was obtained by initial immobilization of $AuCl_4 \cdot 4H_2O$ on Fe_3O_4@COF by electrostatic interaction between amine group and $AuCl_4^-$, followed by reduction of Au(III) to Au NPs using $NaBH_4$ as the reductant. Finally, β-CD functionalized COF (Fe_3O_4@COF@Au-β-CD) was formed by Au-S bonding between Fe_3O_4@COF@Au and thiolated-β-CD.

The final material Fe_3O_4@COF@Au-β-CD (with COF thickness being 25 nm) was exploited for the extraction of nine SAs. The extraction of SAs increased due to hydrogen bonding between hydroxyl groups on the surface of MagCOF and amino groups of SAs. Additionally, the presence of π interaction between phenyl rings, uniform pore structure and the large specific surface area also enhances the extraction efficiency. Besides, hydrophilicity and polarity also played a vital role in extraction process. To check the applicability of this adsorbent, authors studied linearity, LOD, precision and RSDs under optimized conditions. It was found that the proposed method showed good linearity in the range of 2–100 μg kg^{-1} and the LODs were calculated to be 0.8–1.6 μg kg^{-1} (S/N = 3). Moreover, the authors performed extraction process at two kinetic models: pseudo-first-order and pseudo-second-order and it was found that pseudo-second-order kinetic was better fitted with the adsorption kinetics of SAs with R^2 greater than 0.99. Admiringly, the proposed method was magnificently applied for quantification of SAs from real samples. The recoveries were ranged from 78.9 to 112.0%. The fabricated magnetic adsorbent furnished high extraction efficiency of trace SAs under mild conditions.

3.8 Glycopeptides extraction

Glycosylation is considered as one of the most important and complex post-translational modifications.[116] Protein glycosylation plays a vital role in biological activity and bio-synthesis including molecular recognition, protein folding, intracellular transport, fertilization morphogenesis, endocytosis and many others.[117] Meanwhile, both structural and compositional changes in glycosylation are allied with a variety of human diseases, such as autoimmune, breast cancer, hepatocellular carcinoma, prostate cancer and genetic diseases.[118] Therefore, there is a need for the development of a stable and sensitive method for the enrichment of glycopeptides.

Considering the benefits of MagCOFs, Qian and co-workers fabricated Fe_3O_4@TpPa-1 *via* a two-step solvothermal reaction and investigated the efficacy of the material for the hydrophilic enrichment of N-glycopeptides from standard glycoproteins and human serum digests by Hydrophilic interaction chromatography (HILIC) (Fig. 15).[119] To synthesize crystalline keto-enamine linked Fe_3O_4@TpPa-1, initially, Fe_3O_4 (of size 40 nm) were obtained by hydrothermal method. Subsequently, the monomers Tp and Pa were grafted over MNPs through *in situ* solvothermal reaction to acquire MagCOF. The highly ordered 2D topology with nitrogen rich frameworks and amino-terminals enhances the enrichment efficiency for N-glycopeptides. The TEM and SEM images (Fig. 15b and c) show sea-urchin type morphology of the adsorbent, which could provide increased
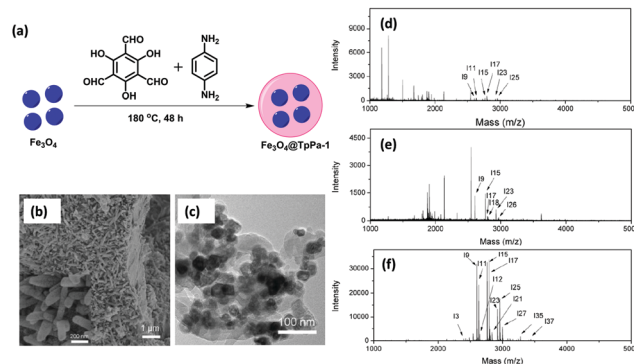

Fig. 15 Schematic illustration of the (a) synthesis of Fe_3O_4@TpPa-1, (b) SEM, (c) TEM image of Fe_3O_4@TpPa-1, MALDI-TOF MS spectra of human IgG digest (70 fmol μL^{-1}) (d) direct analysis, (e) after enrichment by Fe_3O_4 and (f) after enrichment by Fe_3O_4@TpPa-1. Reproduced with permission from ref. 119. Copyright 2017 Royal Society of Chemistry.

specific surface area and available active sites which are highly advantageous for mass transfer and separation processes.

Further, the feasibility of Fe_3O_4@TpPa-1 was checked in the enrichment of N-glycopeptides using tryptic digests of a standard glycoprotein (human IgG). Fig. 15d–f represents that without enrichment, only six peaks of glycopeptides with lower intensities were observed. However, after enrichment with Fe_3O_4@TpPa-1, 37 glycopeptide peaks were analyzed with high MS signal intensities and increased S/N ratio which was higher than previously reported literature. Further the activity of bare MNPs was also tested: only 6 glycopeptide peaks were detected along with the detection sensitivity of Fe_3O_4@TpPa-1 at different concentrations. It was found that upon a decrease in concentration, the number of glycopeptides was decreased. Moreover, the selectivity and specificity test of Fe_3O_4@TpPa-1 was also evaluated using digest mixture of IgG and bovine serum albumin. Results indicated that Fe_3O_4@TpPa-1 showed fast, efficient and selective enrichment of N-glycopeptides. Inspired by the results, the authors also investigated the capability of Fe_3O_4@TpPa-1 in tryptic digests of human serum, which greatly showed identification of 228 glycopeptides corresponding to 114 glycoproteins within three independent replicates which is better than commercial HILIC. The LOD was found to be low (28 fmol) with recoveries of 94.3% and 86.3% for two deglycopeptides.

On a similar note, Deng *et al.* presented a promising approach for the enrichment of endogenous glycopeptides in human saliva by designing hydrophilic MagCOF (mCTpBd) as shown in Fig. 16.[120] The mCTpBd with inherent hydrophilicity has been synthesized by the following procedure: first of all, Fe_3O_4 were synthesized by solvothermal method and to facilitate the growth of COF shell, MNPs were coated with a layer of silica *via* sol–gel approach. Thereafter, to enhance the interaction, amine groups were introduced by surface modification of the silica encapsulated MNPs using APTES (Fe_3O_4-NH_2; 336 nm). Furthermore, Fe_3O_4-NH_2 surface was pre-modified using a monomer, carboxyl-modified 1,3,5-triformylphloroglucinol, CTp *via* amidation reaction (Fe_3O_4-NH_2-CTp), to boost
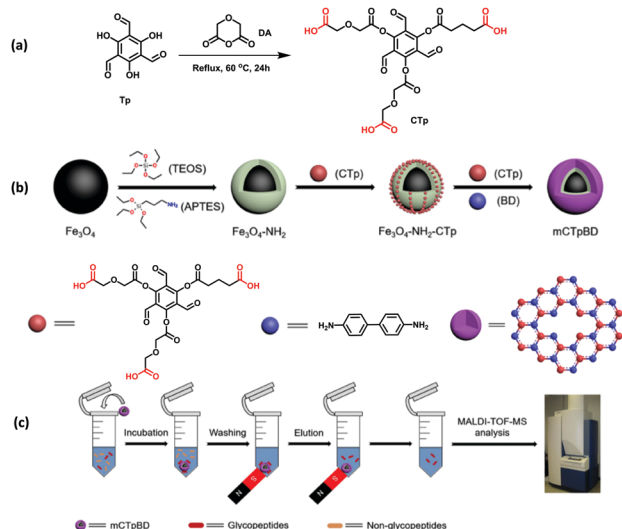
Fig. 16 Synthetic route of mCTpBD and enrichment procedure of glyco-peptides by mCTpBD. Reproduced with permission from ref. 120. Copyright 2020 American Chemical Society.

Fig. 17 (a) Synthetic illustration of the SPIO@COF-guanidyl nanospheres and (b) workflow of the enrichment strategy for phosphopeptides by SPIO@COF-guanidyl nanospheres. Reproduced with permission from ref. 121 Copyright 2020 Elsevier B.V.

the interaction among inorganic magnetic core and organic moieties. Finally, mCTpBd (398 nm; 31 nm COF thickness) was obtained by the reaction between Fe_3O_4-NH_2-CTp and another monomer Bd through interface deposition method with reflux conditions under argon atmosphere. mTpBd was also synthesized in a similar manner.

In order to study the enrichment performance of mCTpBd for glycopeptides, it was first tested for HRP tryptic digest. It was observed that the introduction of mCTpBd greatly enhanced enrichment performance. Before enrichment, only a few of the glycopeptides were observed. Results showed that after enrichment with mTpBd and mCTpBd, the number of glycopeptide peaks were increased. But, enrichment performance of mCTpBd was vastly improved in comparison with mTpBd, revealing the enhanced hydrophilicity obtained from the carboxyl-modified monomer. Further, the adsorption capacity remained nearly intact even after continuous adsorption–desorption cycles. Inspired by the outstanding results of mCTpBd, it was also deployed for the enrichment of glyco-peptides from biological samples (saliva of healthy people and patients with inflammatory bowel disease). Noteworthy, the magnetic adsorbent possessed excellent enrichment capacity in both the cases. Subsequently, mCTpBd with inherent hydrophilicity is a favourable candidate for the enrichment of endogenous glycopeptides.

Another kind of guanidyl-functionalized MagCOF has been synthesized by Wu *et al.* via post synthetic modification using stable precursors including 2,5-divinylterephthalaldehyde and TAPB.[121] These two precursors were reacted along with Superparamagnetic iron oxide nanoparticles (SPIO) to form grafted COF, *i.e.* SPIO@COF. To provide NH_2 functionality, cysteamine was introduced on SPIO@COF by thiol–ene "click" reaction to obtain SPIO@COF@NH_2 nanospheres. As guanidyl is a group having efficient affinity for specific phosphopeptide enrichment,
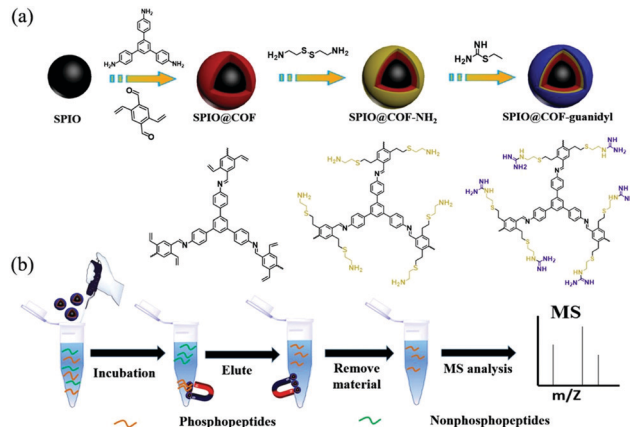
guanidinylation of SPIO@COF@NH_2 nanospheres was carried out using 2-ethyl-2-thiopseudourea hydrobromide to form SPIO@COF-guanidyl nanospheres (20 nm COF thickness) (Fig. 17). The so-formed magnetic adsorbent was used for the selective enrichment of endogenous phosphopeptides from human saliva and analyzed by MALDI-TOF MS. Impressively, due to large surface area, abundant affinity groups, mesoporous structure and excellent magnetic response, SPIO@COF-guanidyl exhibited excellent performance for the selective enrichment of phosphopeptides.

Likewise, Jia *et al.* developed guanidyl-based magnetic ionic COFs (Fe_3O_4@iCOFs) using guanidyl as ionic ligand instead of post synthetic modifications.[122] Fe_3O_4@iCOF was fabricated by immobilizing benzene-1,3,5-tris-carbaldehyde and 1,3-diamino-guanidino hydrochloride on the surface of MNPs (of size 150 nm) through hydrogen bond interactions (Fig. 18). The fabricated magnetic adsorbent was then utilized for selective enrichment of phosphopeptides. The reason behind phosphopeptides enrichment is electrostatic and hydrogen bonding interactions between phosphate and guanidyl groups. By combining with MALDI-TOF MS determinations, Fe_3O_4@iCOFs exhibited good enrichment capacity for phosphopeptides. The developed protocol offered several key advantages such as superparamagnetism,
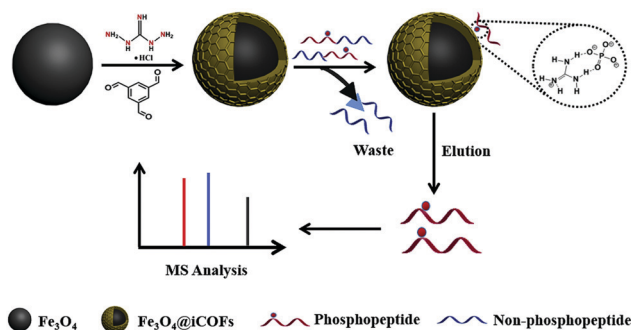
Fig. 18 Synthetic scheme of Fe_3O_4@iCOFs for selective enrichment of phosphopeptides with Fe_3O_4@iCOFs. Reproduced with permission from ref. 122. Copyright 2020 Elsevier B.V.
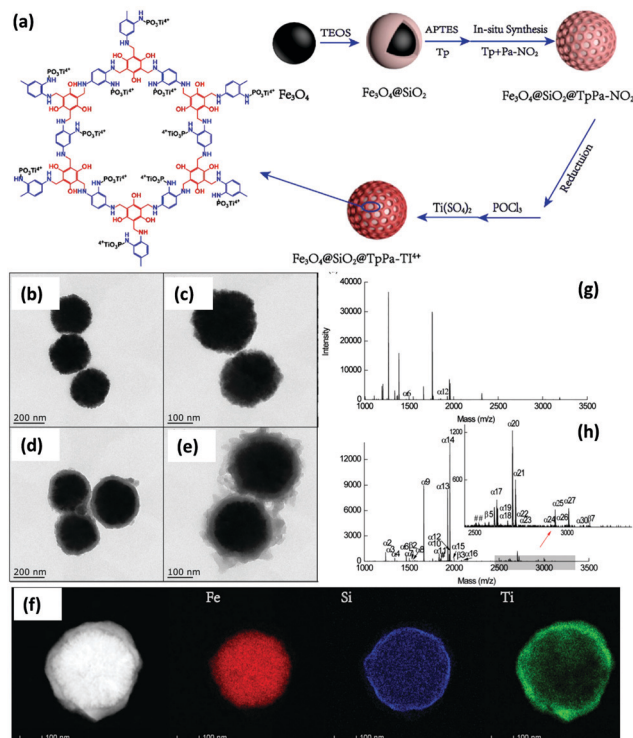
Fig. 19 (a) Synthetic route of Fe$_3$O$_4$@SiO$_2$@TpPa-Ti^{4+} nanoparticles, TEM images of (b) Fe$_3$O$_4$, (c) Fe$_3$O$_4$@SiO$_2$, (d) Fe$_3$O$_4$@SiO$_2$@TpPa-NO$_2$, (e) Fe$_3$O$_4$@SiO$_2$@TpPa-Ti^{4+}, (f) elemental mapping of Fe$_3$O$_4$@SiO$_2$@TpPa-Ti^{4+} (the first image without elemental labelling is high magnification TEM image), MALDI-TOF mass spectra of α-casein (g) before enrichment and (h) after enrichment with Fe$_3$O$_4$@SiO$_2$@TpPa-Ti^{4+}. Reproduced with permission from ref. 123 Copyright 2020 Royal Society of Chemistry.

high sensitivity and selectivity along with recycling up to seven times.

On a similar note, another magnetically recyclable core–shell structure featuring Ti^{4+} functionalized microporous COF was synthesized by Zhang *et al.* The synthesis of Fe$_3$O$_4$@SiO$_2$@TpPa-Ti^{4+} (40 nm COF thickness) is depicted in Fig. 19a wherein MNPs were used as magnetic core and functionalized with silica layer *via* Stöber sol–gel approach.[123] Surface modification of Fe$_3$O$_4$@SiO$_2$ was carried out by introducing amine groups on its surface using APTES. The magnetically retrievable adsorbent could be easily recovered from the reaction mixture and hence, prevented the loss and separation time of adsorbent. Subsequently, Tp, a monomer of COF was immobilized on amino functionalized MNPs to form Fe$_3$O$_4$@SiO$_2$-Tp. In addition, to obtain Fe$_3$O$_4$@SiO$_2$-TpPa-NO$_2$, reversible growth of microporous TpPa-NO$_2$ was performed on Fe$_3$O$_4$@SiO$_2$-Tp. Fe$_3$O$_4$@SiO$_2$-TpPa-NO$_2$ further underwent a reduction in the presence of NaBH$_4$ to convert nitro groups into amino groups for the further phosphate-linking reaction. Also, during the reduction process the imine linkages of COFs were converted into secondary amines, which could provide good hydrophilicity to capture phosphopeptides. Finally, due to strong affinity between phosphates and titanium ions, titanium ions were chelated to phosphates. As shown in Fig. 19b, Fe$_3$O$_4$ nanoparticles displayed

nearly spherical shape with the average particle size of 220 nm. Fig. 19c shows the TEM image of Fe$_3$O$_4$@SiO$_2$ with dark MNP core coated by grey silica shell of ∼20 nm. This silica layer not only protect Fe$_3$O$_4$ from aggregation but also provides sites for the functionalization of amino groups which is necessary for the reversible assembly of covalent organic frameworks. Besides, after *in situ* Schiff-base condensation reaction, a porous covalent organic layer with thickness of 40 nm over Fe$_3$O$_4$@SiO$_2$@TpPa-NO$_2$ nanoparticles was observed (Fig. 19d). Further, TEM images of Fe$_3$O$_4$@SiO$_2$@TpPa-Ti^{4+} and EDX-mapping image of Fe, Si and Ti showed uniform spherical morphology and smooth surface of the synthesized composites and reveals that Ti^{4+} groups were densely grafted into inner channels and surface of COFs (Fig. 19e and f).

The as-synthesized magnetic adsorbent was utilized for selective enrichment of phosphopeptides from bio samples. In this case, tryptic standard phosphoprotein (α-casein) digests are used as model samples to evaluate the phosphopeptide enrichment performance of Fe$_3$O$_4$@SiO$_2$@TpPa-Ti^{4+} composite. Fig. 19g and h demonstrates MALDI-TOF mass spectra of α-casein before enrichment and after enrichment with Fe$_3$O$_4$@SiO$_2$@TpPa-Ti^{4+}. The spectra suggested that only two phosphopeptide peaks (m/z = 1466.7 and 1927.7) were observed before enrichment at very low signal-to-noise ratio and after enrichment with magnetic adsorbent, thirty peaks of phosphopeptides were detected, indicating an excellent performance of so-formed magnetic adsorbent. The selectivity of Fe$_3$O$_4$@SiO$_2$@TpPa-Ti^{4+} was also checked in presence of other samples. The proposed method gave high precision with low LOD, which could be attributed to abundant affinity sites. Also, Fe$_3$O$_4$@SiO$_2$@TpPa-Ti^{4+} showed admirable performance in rat brain lysates with a high specificity of 91.8%.

3.9 Marine biotoxins extraction

Marine biotoxins are produced by aquatic micro-organisms and accumulate in filter-feeding shellfish mussels, clams, oysters or scallops, creating a public health risk.[124] These toxins enter the human body through inhalation and by consumption of contaminated seafood. However, okadaic acid (OA) and dinophysistoxin-1 (DTX-1), a group of marine biotoxin, are lipophilic heat-stable toxins which are produced by marine dinoflagellates.[125] They pose a serious threat to human health, *e.g.* gastrointestinal syndrome, such as diarrhetic shellfish poisoning (DSP). In addition, after monitoring the concentration of these biotoxins, it was found that their concentration level is very low in seawater ($\leq$ng L^{-1}). Therefore, preconcentration of OA and DTX-1 is required prior to detection.[75]

In view of this, Salonen *et al.* performed extraction of OA and DTX-1 from sea-water in the presence of magnetically retrievable crystalline COF (mTpBd-Me$_2$).[75] To obtain mTpBd-Me$_2$, a controllable simplified three-step procedure was carried out. Firstly, amino-functionalized MNPs were obtained by co-precipitation method by introducing dopamine as capping agent (Fe$_3$O$_4$@DOPA; 5 nm). Secondly, a monomer Tp was pre-functionalized on the surface of Fe$_3$O$_4$@DOPA (Fe$_3$O$_4$@DOPA-Tp); pre-grafting facilitates the nucleation and growth of COF shells around
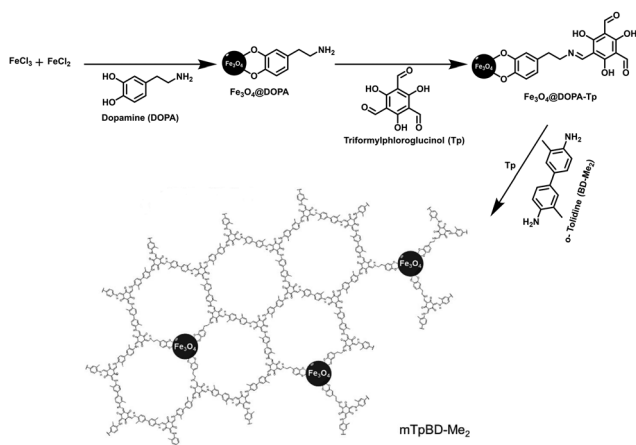
Fig. 20 The three-step synthesis of mTpBD-Me$_2$. Reproduced with permission from ref. 75. Copyright 2019 Royal Society of Chemistry.

Fig. 21 Schematic diagram for the synthesis of M–COF–SH. Reproduced with permission from ref. 131. Copyright 2020 Elsevier B.V.

dopamine functionalized MNPs. Lastly, to grow mTpBd-Me$_2$, another COF monomer, di-methyl benzidine (Bd-Me$_2$) and Tp/o-tolidine in a 1:1.5 molar ratio was exposed on the pre-functionalized MNPs in the presence of acetic acid as catalyst (Fig. 20). Noteworthy, non-pre-grafted Fe$_3$O$_4$@DOPA led to amorphous COFs.

The optimal concentration for the synthesis of mTpBd-Me$_2$ was tested with the amount of Tp ranging from 0.005 to 0.4 mmol. Further, 0.1, 0.2 and 0.4 mmol yielded crystalline composites such as 0.1-mTpBd-Me$_2$, 0.2-mTpBd-Me$_2$ and 0.4-mTpBd-Me$_2$. In addition, 0.2-mTpBd-Me$_2$ was selected for the extraction of OA and DTX-1 due to their high organic content and stability up to 380 °C. The kinetic studies showed fast adsorption due to presence of large surface of the nanocomposite. Moreover, the adsorption isotherm for both the biotoxins displayed $n > 1$, demonstrating favourable adsorption. Furthermore, a good adsorption capacity of the sorbent was found to be 26.363 mg$^{0.219}$ g^{-1} L$^{0.781}$ and 22.508 mg$^{0.181}$ g^{-1} L$^{0.819}$ for OA and DTX-1, respectively, which was indicated by K_F (indicator of adsorption capacity in Freundlich theory) value. Additionally, the maximum adsorption capacity was calculated to be 812 mg g^{-1} for OA and 830 mg g^{-1} for DTX-1, which was three-fold higher for OA as compared to bulk TpBd-Me$_2$. Also, mTpBd-Me$_2$ exhibited higher calculated adsorption kinetics, *i.e.*, ∼500-fold increase for OA and ∼300-fold increase for DTX-1 as compared with literature precedents. This increase can be attributed to the ordered pore structure of MagCOFs which allows higher diffusion rates for bio-toxins instead of non-magnetic bulk COFs which are difficult to separate from sample matrix. Besides, the recyclability efficiency of the adsorbent was also examined and was found that the adsorbent could be reused for at least five consecutive cycles. Consequently, mTpBd-Me$_2$ had good potential for rapid extraction of marine biotoxins from sea water. The adsorption and concentration of other pollutants such as pesticides and detoxification of other bio-toxins can also be studied using mTpBd-Me$_2$ as adsorbent. Moreover, routine monitoring of OA and DTX-1 in sea water is essential to avoid shellfish contamination.
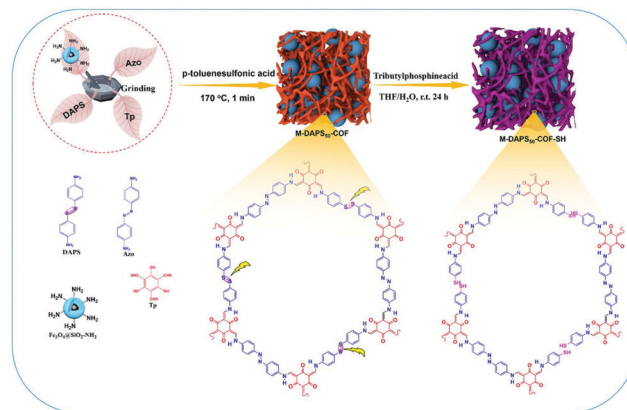
3.10 Metal ions extraction

Rapid pace of industrialization, population expansion and urbanization have significantly deteriorated the quality of water.[126,127] Heavy metal ions, which are discharged into the water bodies through various effluents, are very fatal to the human health and surrounding environment as they tend to bioaccumulate through food chain.[128,129] Amongst all, mercury has been identified as one of the most hazardous environmental pollutants, exposure to which causes severe adverse health effects.[130] Hence, its periodic monitoring is imperative. In this respect, Shuai and co-workers reported thiol-functionalized MagCOFs, namely M-DAPS-$_{50}$-COF-SH, *via* salt-mediated crystallization approach and cutting strategy (cutting of disulfide linkages) for selective and efficient removal of Hg^{2+} (Fig. 21).[131]

Subsequently, three M-DAPS-COFs with three different molar ratios (0%, 50% and 100%) of DAPS were synthesized. Remarkably, amongst all, M-DAPS$_{50}$-COF was obtained in high yield (∼95%). It contains densely distributed thioether side chains as the Hg^{2+} receptor due to strong soft-soft interaction between sulfide and mercury. Impressively, Mag-COF-SH showed maximum adsorption capacity of Hg^{2+} (383 mg g^{-1}) which can be attributed to the abundant thiol functional groups and ultra-porous structure of the framework. The selectivity towards Hg^{2+} detection was also checked in presence of other competitive metal ions and satisfactory results were obtained. Moreover, resulting composite exhibited rapid kinetics, *i.e.*, adsorption equilibrium can be achieved within 10 min, which was attributed to high specific surface area of MagCOF composite and strong affinity between thiol (–SH) moieties and Hg^{2+}. Additionally, to evaluate the disconnection of disulfide linkages, integration of MNPs over COF and formation of imine bonds, XPS, XRD and FT-IR spectra were studied, which illustrates satisfactory results. Besides, Mag-COF-SH could be reused up to five adsorption cycles which proposed its use in large scale metal sensing and removal applications.

Chromium is extensively used in various industries including electroplating, leather tanning, metal finishing, pigment synthesis, petroleum refining, *etc.* Two stable forms of chromium exist in environment, trivalent Cr^{3+} and hexavalent Cr^{6+}.
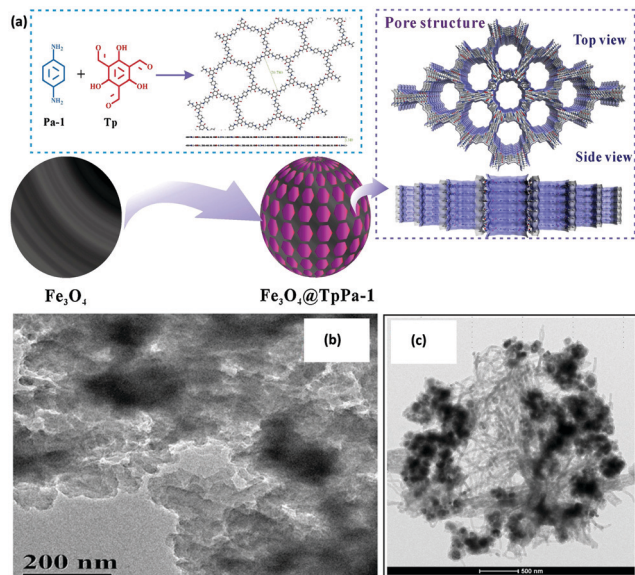
Fig. 22 (a) Synthesis process of core–shell structured Fe₃O₄@TpPa-1, TEM image of (b) TpPa-1 and (c) Fe₃O₄@TpPa-1. Reproduced with permission from ref. 133. Copyright 2020 Elsevier B.V.

However, Cr^{6+} is considered as more hazardous due to its high mobility and solubility in water and soil. Owing to its greater penetration, it can severely affect central nervous system and is a classified carcinogen due to its oxidizing nature.[132] Besides chromium, BPA is also a known pollutant which was discussed thoroughly in the previous section.

In view of this, Hu *et al.* performed removal of Cr^{6+} and BPA from aqueous solution using magnetically retrievable COF (Fe₃O₄@COF; TpPa-1 thickness being 10 nm) with β-keto-enamine linkage under solvothermal reaction conditions (Fig. 22a).[133] The as-synthesized magnetic adsorbent reflected numerous advantages such as simple preparation method, excellent adsorption performance, high stability and good recoverability (19.5 emu g⁻¹). TEM images of TpPa-1 and Fe₃O₄@TpPa-1 illustrate sea-urchin type and spherical morphology with an average diameter of ∼80–100 nm, respectively (Fig. 22b and c). The effect of pH, ionic strength and adsorption isotherms are the key factors in the extraction process. The thermodynamic as well as kinetic studies validate to the pseudo-second-order and Langmuir isotherm indicating spontaneous, endothermic and chemisorption process. The mechanism of BPA extraction follows π–π stacking interaction, hydrogen-bond and porosity induced by hydrophobicity. Moreover, for Cr^{6+} adsorption, firstly anionic Cr^{6+} was combined with the surface protonated functional groups of TpPa-1. Secondly, Cr^{6+} was reduced to Cr^{3+} with the aid of adjacent electron donor groups. Finally, reduced Cr^{3+} was returned into solution due to electronic repulsion. The adsorption capacities for Cr^{6+} and BPA were measured to be 245.45 mg g⁻¹ and 1220.97 mg g⁻¹, respectively. Additionally, magnetic adsorbent was reused for five adsorption–desorption cycles. Nevertheless, there exists certain fundamental aspects which needs to be focused. In our view, influence of different coexisting anions in

adsorption behaviours of Cr^{3+} and Cr^{6+} should be studied to improve the effectiveness of the process. Further, present strategies mainly target the batch extraction, however, continual removal of Cr^{6+} from industrial effluents is more useful as effluents mainly originate from industries involved in production of large amounts of waste.

3.11 Nitro explosive extraction

Recently, several researchers have begun exploring the potential of MagCOFs as chemo-sensory materials due to their exceptional structural tunability and properties. In that context, selective and sensitive detection of nitroaromatic explosives, in particular 2,4,6 trinitrophenol (TNP), has gained tremendous attention due to its detrimental effects on humans, wildlife and environmental health.[134] On similar account, Gao *et al.* designed and fabricated a fluorescent sensor which was composed of MagCOFs, Molecularly imprinted polymers (MIP) and carbon dots (CDs).[135] Fig. 23 illustrates the synthetic protocol of magnetic sensor (MagCOF@MIP@CD) wherein 2,3,5,6-tetrafluoroterephthalaldehyde and TAPB were covalently immobilized over MNPs (of size 200 nm) to form MagCOF. After its successful fabrication, MIP (as selective sorbent) and CDs (as fluorescent sensor) were grafted over MagCOF *via* reverse microemulsion method using APTES as –NH₂ provider and TEOS as cross-linker.

The fabricated MagCOF@MIP@CD was further utilized as a fluorescent sensor for environmental pollutant TNP. The maximum excitation and emission wavelength were recorded to be 370 nm and 470 nm, respectively. MagCOF@MIP@CD without TNP exhibited strong fluorescence signal which was quenched in presence of TNP. Amongst various competitive compounds of TNPs and metal ions, best selectivity was obtained for TNP due to the effective π–π interaction and hydrophobic effect
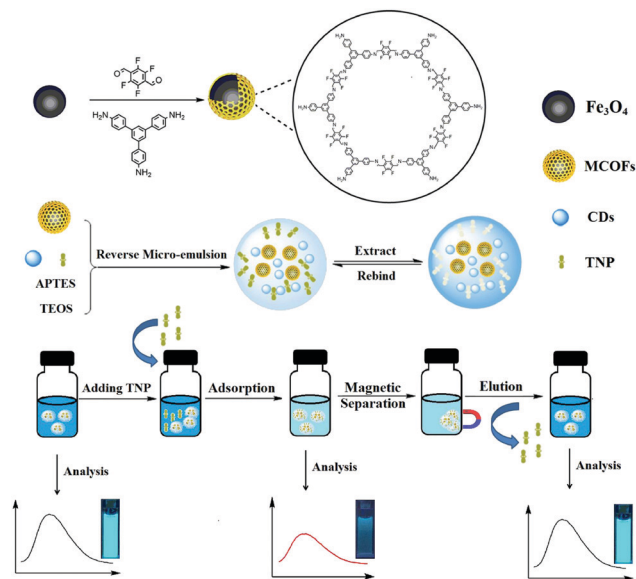

Fig. 23 Synthesis and application of MagCOFs@MIPs@CDs as fluorescent sensor. Reproduced with permission from ref. 135. Copyright 2020 Elsevier B.V.

© 2022 The Author(s). Published by the Royal Society of Chemistry

between TNP with MagCOF@MIP@CD. Hence, MagCOF@ MIP@CD not only provided excellent magnetism and good fluorescence but also exhibited good sensitivity with high imprinting factor (8.4) and shorter detection time (within 1 min). Delightedly, good recoveries (88.7% to 103.4%) were obtained when the fluorescent sensor was applied in real samples. Moreover, recyclability of the sensor up to eight consecutive runs also imparted green credentials for their use at large scale.

Along with nitroaromatic explosives, selective and sensitive detection of endocrine disruptor, PAHs and many more organic pollutants have raised incredible attention due to their adverse effects on aquatic ecosystems, humans and environmental health (Fig. 24).[136] Also, cigarette smoke is composed of various chemicals including gaseous nicotine and tar which have carcinogenic effect on human health. Inhaling such toxic chemicals, Bap and phenols, may cause cancer and many other diseases.[137,138] Therefore, adsorption and removal of these organic pollutants are of great necessity. To fulfil current needs, Zhang *et al.* synthesized novel porous aromatic framework (PAF) decorated MNPs, PAF-6 MNPs, using cyanuric chloride for triangular planar basis and piperazine as linker unit *via* one-step polymerization process as shown in Fig. 25.[139] Zhang developed this sample pre-treatment method by coupling of MSPE with HPLC-UV for the adsorption of TNP, 3-nitro-chlorobenzene, BPA, naphthalene and naphthol from well-water, tap-water, waste water and yellow river water.

The presence of aromatic units and nitrogen atoms provides them multiple recognition sites. The fabricated Porous aromatic framework-6 (PAF-6) MNPs showed remarkable adsorption capability due to presence of π–π interactions, hydrogen-bond interactions and inclusion complexation. TEM image of PAF-6 MNPs showed spherical core–shell structure with narrow size distribution (Fig. 25b). Moreover, PAF-6 MNPs were also used to identify toxicants present in cigarette smoke such as phenolic compounds (*o,m,p*-cresol, phenol, pyrocatechol, resorcinol and hydroquinone), Bap and tar. The results showed that upon increasing the amount of PAF-6 MNPs from 5 mg to 20 mg, the removal efficiencies increased rapidly (Fig. 25c and d). The method showed maximum adsorption capacity (166.85 mg g^{-1}), good linearity for different organic pollutants in the range of 0.01–12 μg mL^{-1} and the R^2 was more than 0.97; the LODs were between 0.083 and 5.020 according to the three-fold signal to
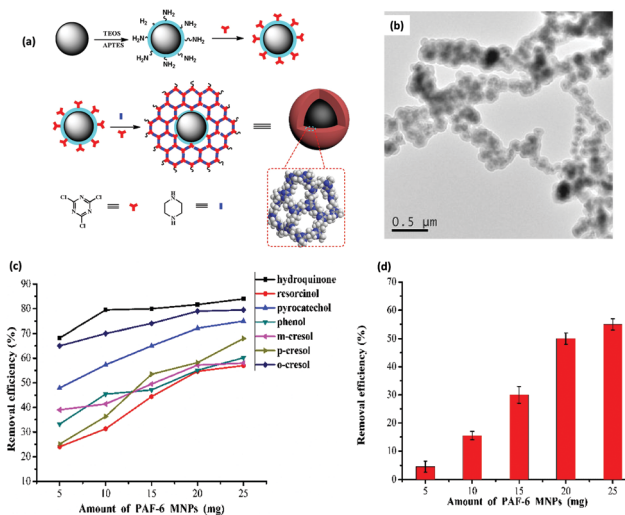

Fig. 25 (a) Preparation procedure of core−shell microspheres (PAF-6 MNPs), (b) TEM image of PAF-6 MNPs and (c) effect of PAF-6 MNPs levels on the removal efficiency of phenolic compounds from cigarette smoke and (d) effect of PAF-6 MNPs dosage on the removal efficiency of Bap from cigarette smoke. Reproduced with permission from ref. 139. Copyright 2018 Elsevier B.V.

noise ratio. The extraction efficiency of the method was in between 84.0% and 96.0% with reusability of at least six cycles. These magnetic porous composites exhibited high stability, desirable durability and enhanced magnetic separation. The results proved that PAF-6 MNPs displayed outstanding adsorption performance for diverse multi target analytes, nitrosamines, heavy metal ions and other toxic compounds.

3.12 Phthalate esters extraction

Phthalate Esters Extraction (PAEs) are widely used as plasticizers and additives in many plastics, pesticides and paints. However, they tend to leach into various environmental matrices and eventually migrate to humans. PAEs cause adverse effects on human health such as carcinogenicity and endocrine disruption.[140,141] On this note, MagCOF (COF-(TpBd)/Fe$_3$O$_4$) was designed by Pang *et al.* for efficient extraction of PAEs in beverage samples.[142] Fig. 26a depicts the magnetic adsorbent synthetic protocol and SPE of PAEs wherein COF-(TpBd) was synthesized by conventional solvothermal method through Schiff base condensation reaction between monomers Tp and Bd. Further, the obtained COF-(TpBd) was delaminated into COF nanosheets *via* mechanochemical grinding. The as-synthesized COF-(TpBd) nanosheets were further anchored on the surface of MNPs (of size <50 nm) through co-precipitation method to form COF-(TpBd)/Fe$_3$O$_4$. The designed magnetic adsorbent was successfully utilized for extraction of 15 PAEs and displayed excellent extraction efficacy (Fig. 26b). The authors also compared the previously reported methods for PAEs detection. The results endowed that our developed method showed great significance in extraction of PAEs due to hydrophobic effect, π–π interactions and pore size selectivity between PAEs (8 Å to 17 Å) and COF-(TpBd)/Fe$_3$O$_4$ (24 Å). Moreover, under optimized conditions, a
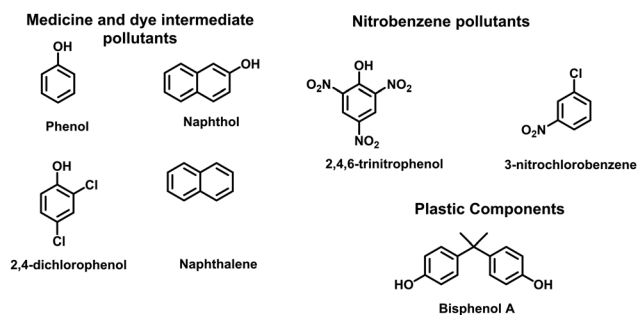

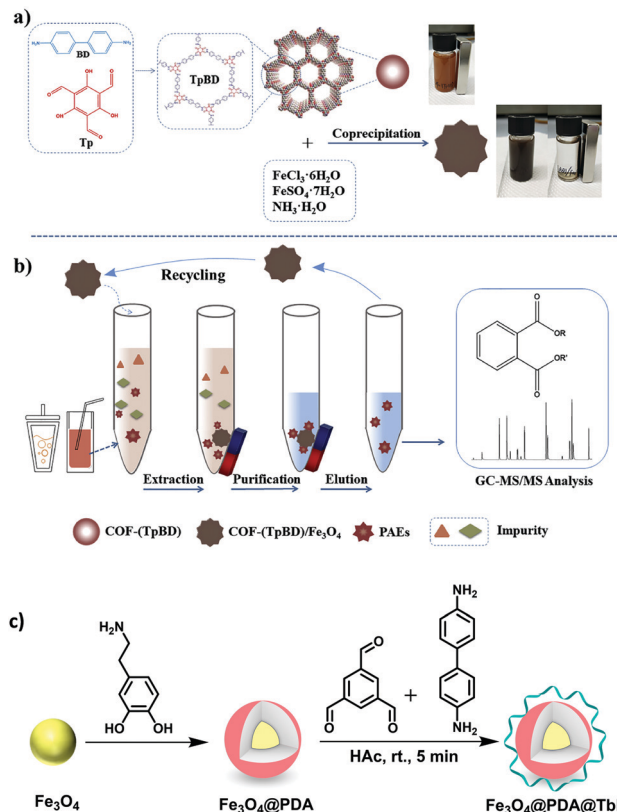Fig. 24 Structures of a few emerging organic micropollutant.

Fig. 26 Schematic diagram for (a) magnetization of COF-(TpBD), (b) application of COF-(TpBD)/Fe₃O₄ as absorbent for MSPE and detection of PAEs. Reproduced with ref. 142, Copyright 2020 Elsevier B.V. (c) Synthesis of Fe₃O₄@PDA@TbBd.

Fig. 27 (a) Schematic representation for the preparation of Fe_3O_4/C-COP, (b) proposed adsorption mechanism of AO/RB onto Fe_3O_4/C-COP and (c) VSM curves of Fe_3O_4 and Fe_3O_4/C-COP before and after AO and RB adsorption, (d) regeneration studies of magnetic Fe_3O_4/C-COP using ethanol and (e) N_2 adsorption/desorption isotherm of Fe_3O_4/C-COP before (a) and after (b) AO and RB adsorption Reproduced with permission from ref. 147. Copyright 2020 American Chemical Society.

series of analytical parameters were thoroughly studied. The proposed approach possessed a good linear range (10–1000 µg L⁻¹) with $R^2 > 0.9912$. The LOD and LOQ were from 0.005 to 2.748 µg L⁻¹ and from 0.018 to 9.151 µg L⁻¹, respectively with lower RSDs. In addition, to check the accuracy of the method, COF-(TpBd)/Fe₃O₄ was applied in recognition of PAEs from real samples. The method showed good recoveries in the range of 79.3–121.8% and RSDs values were within 2.1–11.9%. Last but not the least, magnetic adsorbent was reused for four cycles.

Similarly, Liang and co-workers fabricated MagCOFs by Schiff base condensation reaction of two monomers Tb and Bd on PDA functionalized Fe₃O₄ (Fig. 26c).[143] In this case, PDA was used as a hydrophilic middle layer which displayed excellent water dispersibility and good biocompatibility. The synthesized adsorbent exhibited several advantages including high surface area, large number of active sites for PAEs detection (via π–π and hydrophobic interactions), easy separability and high aqueous dispersibility. The fabricated magnetic adsorbent was further deployed for recognition of nine PAEs from a human plasma sample. Favourably, Fe₃O₄@PDA@TbBd unveiled great potential in PAEs detection with wide linearity (50–8000 ng mL⁻¹) and low LOD (0.0025–0.01 ng mL⁻¹). The proposed strategy showed good recovery (92.3–98.9%) and a small RSD value (for intra-day <4.6% and for inter-day <6.8%). To check the superiority of the adsorbent it was applied in real sample analysis
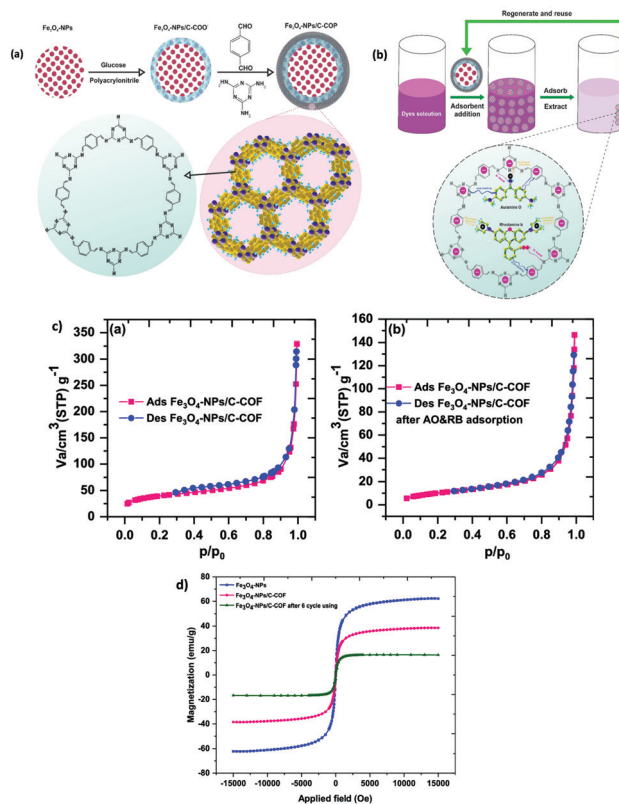
and favourable results were obtained. Besides, the adsorbent was magnetically recovered and used repeatedly for five cycles.

3.13 Aromatic dyes removal

Aromatic dyes represent a substantial class of pollutants due to their unfavourable effects on human and wildlife such as carcinogenicity, teratogenicity and mutagenicity.[144] Among aromatic dyes, auramine O (AO) has been used for colouring paper, textile, leather and rhodamine (RB) have been utilized for industrial purposes.[145,146] These aromatic dyes are substances of concern for the environment and human health as they create gastrointestinal and respiratory tract irritation. Therefore, their removal is of great significance for researchers.

Recently, Rafiee and co-workers fabricated a melamine-rich magnetic covalent organic polymer (MCOP) for the removal of AO and RB.[147] Fig. 27a depicts the fabrication of the MCOP wherein MNPs (of sizes 20–50 nm) were synthesized by solvothermal technique. Surface modification of MNPs using glucose and polyacrylonitrile provided carboxylate units which ease the COP coverage easily onto Fe₃O₄. The final adsorbent (Fe₃O₄/C-COP) was formed by Schiff base condensation reaction between TPA and melamine on the surface of modified MNPs. Fig. 27b represents the mechanistic pathway for the

removal of AO and RB. The presence of free lone pair electron in various imine groups present on Fe_3O_4/C-COP could electrostatically interact with cationic RB and AO, which enhanced the adsorption behaviour. Also, due to the planar structure of the dye it can be readily adsorbed on the adsorbent through hydrogen-bonding and van der Waals forces. Brunauer–Emmett–Teller (BET) surface area and Barrett–Joyner–Halenda (BJH) pore-size analyses confirmed the cavity encapsulation. The surface area and pore volume of Fe_3O_4/C-COP before and after adsorption was determined by BET analysis (Fig. 27c). The surface area and pore-volume before adsorption was calculated to be 150.51 $m^2 g^{-1}$ and 0.4125 $cm^3 g^{-1}$, respectively whereas after adsorption of AO and RB both surface area (38.89 $m^2 g^{-1}$) and pore-volume (0.2191 $cm^3 g^{-1}$) decreased. The decrease in values was due to encapsulation of AO and RB in the cavity. The authors also compared the results with previously reported adsorbents, which revealed better results in terms of mass (12 mg) and contact time (4 min). The maximum adsorption capacity for AO and RB were 107.11 and 131.23 $mg g^{-1}$, respectively. The higher maximum adsorption capacity value for RB is attributed to the π–π interactions mechanism between RB and the material.

From VSM analysis, the saturation magnetization value for Fe_3O_4/C-COP was observed to be 37.5 $emu g^{-1}$ which is lower than the magnetization of bare Fe_3O_4 (81.5 $emu g^{-1}$). Fig. 27d shows that M_s value of Fe_3O_4/C-COP after six cycles was found to be lower after AO and RB adsorption than the fresh Fe_3O_4/C-COP. This reduction in the saturation magnetization can be attributed to the fact that with the addition of AO and RB to Fe_3O_4/C-COP the surface magnetic anisotropy of magnetite changes which leads to an increase in surface spin disorientation. This results in the decrease of magnetic moment of the adsorbent and hence decrease in M_s value of Fe_3O_4/C-COP. Besides, due to simple magnetic recoverability, the adsorbent was reused for nine consecutive cycles.

3.14 Fluoroquinolones extraction

Fluoroquinolones (FQs) possess strong anti-bacterial activity for both pathogenic Gram-positive and Gram-negative bacteria.[156,157] Due to their excellent activity they have been widely used in the field of farming, clinical practice and aquaculture. However, their overdose can result in residues in foodstuffs in humans and animal origin. Also, the extensive usage of FQs led to many toxic effects such as pathogen resistance and allergic reactions in human beings. Therefore, there is a need to develop feasible method to inspect FQs residues.

In this regard, Gao and co-workers fabricated core–shell structured MagCOFs for the efficient extraction of six FQs (ciprofloxacin, enrofloxacin, lomefloxacin, gatifloxacin, levofloxacin and pefloxacin) from pork, milk and human plasma through MSPE coupled HPLC technique (Fig. 28a).[158] The MagCOF was synthesized by immobilizing 4,4''-diamino-p-terphenyl and 1,3,5-tris(p-formylphenyl) benzene onto Fe_3O_4 by Schiff base condensation reaction. The new magnetic adsorbent exhibited low density, high surface area, excellent porosity, high thermal stability and offered effortless magnetic separability. Moreover, VSM studies revealed that Fe_3O_4@COFs
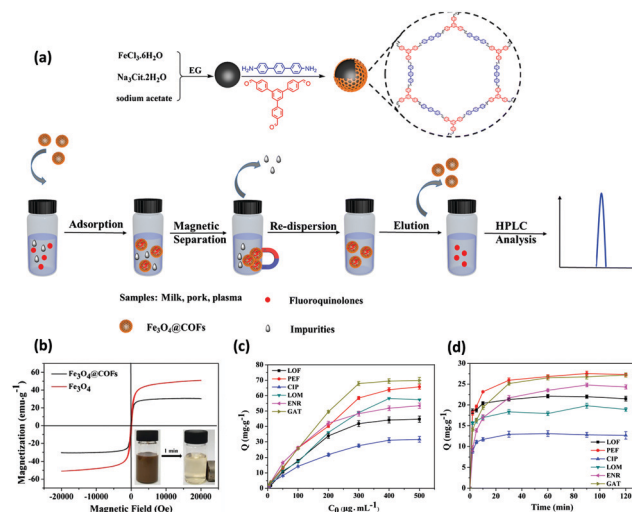

Fig. 28 (a) Synthesis and application of Fe_3O_4@COFs, (b) VSM studies of Fe_3O_4, (c) adsorption isotherms of six FQs on Fe_3O_4@COFs and (d) adsorption kinetics of six FQs on Fe_3O_4@COFs. Reproduced with permission from ref. 158 Copyright 2019 Springer Nature Publishing AG.

display excellent magnetization (36 $emu g^{-1}$) (Fig. 28b). To check the feasibility of MagCOF, adsorption kinetics and isotherms were obtained. Fig. 28c depicts the saturation adsorption capacities of six FQs $i.e.$, as the concentration of FQ in the solution increases, adsorption of FQ on Fe_3O_4@COFs increases whilst Fig. 28d demonstrates that adsorption capacities were gradually increased in the initial 30 min and after 30 min adsorption kinetic curves are flat. These results suggest that adsorption equilibria was achieved in 30 min. Furthermore, from adsorption isotherms it was noted that Freundlich isotherm was better fitted in FQs adsorption, indicating that the adsorption process is not caused by monolayer, but by various interactions. The adsorption mechanism of MagCOF to FQs was mainly attributed to hydrogen bonding and π–π interaction between phenyl rings. Further, under optimized conditions (sorbents dosage, extraction time, pH of samples solution, ionic strength, $etc.$) analytical performance was investigated. The MSPE coupled HPLC analysis presented wide linear range (2.5–1500 $ng g^{-1}$), low LOD (0.5 $ng g^{-1}$) with $R^2 > 0.9996$. The method showed good recoveries (78.7–103.5%) in milk, pork and human plasma/actual samples with RSDs ranging from 1.5 to 4.3% for intra-day and 2.9% to 6.2% for inter-day. Besides, Fe_3O_4@COFs could be reused for ten adsorption–desorption cycles.

Similarly, Li $et al.$ synthesized sulfonate-functionalized Mag-COF for the effective extraction of FQs in food samples through MSPE-HPLC-MS/MS method (Fig. 29).[154] For the preparation, firstly Fe_3O_4 NPs were modified by Schiff base reaction between Tp and Bd. Further, Fe_3O_4@TpBd-Au was fabricated by loading gold nanoparticles on Fe_3O_4@TpBd. Furthermore, Fe_3O_4@TpBd-Au was functionalized by immobilization of sodium 3-mercaptopropanesulphonate via Au–S bond formation. The adsorption of FQs is attributed to the strong π–π stacking, hydrogen bonding and electrostatic interactions. The proposed method showed linearity with excellent R^2 value (≥ 0.9989) and lower LOD (0.1–1.0 $\mu g kg^{-1}$). Moreover, the method displayed

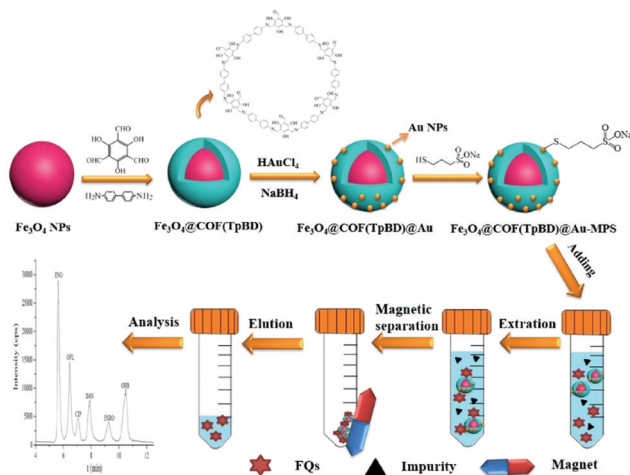**Fig. 29** Schematic fabrication process of Fe$_3$O$_4$@COF(TpBD)@Au-MPS and the MSPE procedure for the determination of FQs. Reproduced with permission from ref. 154. Copyright 2020 Elsevier B.V.

satisfactory recoveries (82–110.2%) in food stuffs with lower RSDs. The as-synthesized magnetic adsorbent showed superior adsorption ability and magnificent chemical stability. Adsorption performance and structural parameters of variety of COFs have been listed in Table 2.

3.15 Estrogen enrichment

Estrogens are widely used in oral contraceptive and hormone therapy which are chiefly involved in reproduction, growth and sexual behaviour. Recently, due to potential risk on human health and environment their widespread use has gained considerable attention.[162,163] Therefore, determination of estrogens in complex samples is very important from both environmental and humanitarian grounds. In this regard, Lin and co-workers reported the first example of MagCOF nanobeads (Fe$_3$O$_4$@TbBd) and explored it as an adsorbent for MSPE of estrogens from human urine samples followed by HPLC-MS analysis (Fig. 30).[155] Due to the complex matrix effect and because of ultra-low concentration of estrogens in biological samples, pretreatment and enrichment processes are imperative prior to HPLC-MS. The core–shell structured MagCOF (Fe$_3$O$_4$@TbBd) nanobeads were synthesized by Schiff base condensation reaction of monomers Tb and Bd in the presence of DMSO on the surface of Fe$_3$O$_4$ at room temperature. The superior utility of Fe$_3$O$_4$@TbBd was demonstrated by some of their attractive features such as large specific surface area (202.18 m^2 g^{-1}), excellent chemical and thermal stability, high porosity (2.8 nm) and high magnetic responsivity (41.4 emu g^{-1}), which made them an ideal adsorbent for selective separation and enrichment of estrogens. Moreover, TEM images indicated uniform size and monodispersity of bare Fe$_3$O$_4$ ($\sim$200 nm) and distinct core–shell structure of Fe$_3$O$_4$@TbBd nanobeads with dark Fe$_3$O$_4$ NPs core and gray COF layer with thickness of 40 nm (Fig. 30c and d). The as-synthesized Fe$_3$O$_4$@TbBd@COF was characterized by various physio-chemical techniques. Moreover, a simple and sensitive method was developed by combination of MSPE with HPLC-MS by using Fe$_3$O$_4$@TpBd nanobeads, which displayed LOD (0.2–7.7 ng L^{-1}, (S/N = 3)), good linearity

Table 2 Adsorption performance and structural parameters of MagCOFs

| MagCOF	Adsorption time (min)	Desorption time (min)	Adsorption dosage (mg)	Elution solvent	Surface area (m^2 g^{-1})	Pore volume (cm^3 g^{-1})	Pore size	Ref.
Fe$_3$O$_4$@COF	30	3	40	Methanol	166.5	0.26	n.d.	148
NiFe$_2$O$_4$@COFs	5	n.d.	10	Acetonitrile:methanol	169.7	0.276	n.d.	159
Fe$_3$O$_4$@TpBd	5	1	n.d.	Ethanol	272.6	0.457	1.7 nm	67
Fe$_3$O$_4$@COF	10	2	20	i-Propanol	181.36	0.45	3.6 nm	70
Fe$_3$O$_4$@COFs-Apt	30	n.d.	30	Hexane	185	n.d.	n.d.	36
Magnetic TpPa-1	n.d.	n.d.	5	Acetonitrile	247.8	0.40	0.4–2.0 nm	71
COF-LZU1@PEI@Fe$_3$O$_4$	30	3	5	Acetonitrile	n.d.	n.d.	n.d.	160
MOPs	20	10	5	Ethyl acetate	378	n.d.	n.d.	
Mag-COF-2	20	n.d.	0.1	Methanol	334.9	0.32	3.9 nm	149
MagCOF	50-DCF 80-SMT	n.d.	10	Acetonitrile	2245	n.d.	2.5 nm	108
Mag-COF-1	60 min	5	5	Acetonitrile	n.d.	n.d.		41
Fe$_3$O$_4$@COF	20	2	10	Acetonitrile	30.6	0.187	2–5 nm	114
Fe$_3$O$_4$@COF@Au-β-CD	30	10	20	Acetonitrile-acetic acid	n.d.	n.d.	n.d.	150
Fe$_3$O$_4$@TpPa-1	30	10	0.02	Acetonitrile-H$_2$O-TFA	186	0.17	3.6 nm	119
mCTpBd	30	30	0.2	Acetonitrile-H$_2$O-TFA	120.41	n.d.	1.3 nm	120
SPIO@COF-guanidyl	30	10	10	Acetonitrile-H$_2$O-TFA	149.75	n.d.	3.2 nm	121
Fe$_3$O$_4$@iCOFs	30	15	5	Acetonitrile-H$_2$O	7	n.d.	n.d.	122
Fe$_3$O$_4$@SiO$_2$@TpPa-Ti^{4+}	30	10	1	Acetonitrile-TFA	128	n.d.	1.4 nm	123
mTpBd-Me$_2$	60	4 h	n.d.	2-Propanol	538	0.40	1.1 nm	152
M-DAPS-COF-SH	10	n.d.	5	HCl and thiourea	181.5	0.24	n.d.	131
Fe$_3$O$_4$@COF(TpPa-1)	10-BPA 100-Cr	n.d.	5	Ethanol	485.2	0.34	2 nm	153
MagCOF@MIP@CD	30	2	0.5	Methanol:acetic acid	137.34	n.d.	4.72 nm	151
PAF-6 MNPs	5	5	60	Acetonitrile	120.2	n.d.	2–5 nm	161
COF-(TpBd)/Fe$_3$O$_4$	30	15	30	Methanol	n.d.	n.d.	n.d.	142
Fe$_3$O$_4$/C-COP	2	4	12	Ethanol	150.51	0.4125	n.d.	147
Fe$_3$O$_4$@COFs	60	20	14	Methanol	124	0.386	3.1 nm	158
Fe$_3$O$_4$@COF(TpBD)@Au-MPS	30	25	20	Formic acid:methanol	70.14	0.15	n.d.	154
Fe$_3$O$_4$@TbBd	30	2	20	Acetonitrile	202.18	0.65	2.8 nm	155
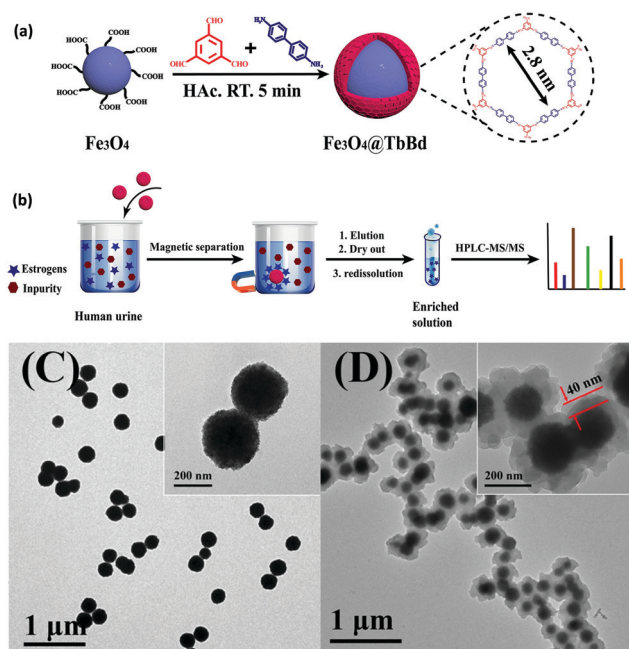
Fig. 30 (a) Preparation of Fe_3O_4@TbBd nanobeads, (b) MSPE process for estrogens in urine samples, TEM images of (c) bare Fe_3O_4 NPs and (d) Fe_3O_4@TbBd nanobeads. Reproduced with permission from ref. 155. Copyright 2018 Elsevier B.V.

($R > 0.9978$), LOQ (0.6–25.6 ng L^{-1}, S/N = 10), high enrichment (75–197-fold) as well as excellent recoverability. Also, the proposed method was used for the analysis of trace estrogens in urine samples of pregnant women and showed good recoveries (80.6–11.6%). Fe_3O_4@TpBd can be reused up to ten adsorption–desorption cycles which proposed its use in large scale extraction and as a novel adsorbent in sample pre-treatment.

4. Comparison with other magnetic materials

Till date, a variety of homogenous and heterogeneous adsorbents have developed for extraction of various organic and inorganic pollutants from different solutions. But, now a days, the use of magnetic adsorbents has gained tremendous attention due to their efficient recyclability, excellent stability and enhanced functionality. Table 3 summarizes the comparative data of MagCOFs with other magnetic adsorbents.

5. Conclusion and future outlook

In the past few years, COFs have gained tremendous attention in the field of separation science due to their magnificent

Table 3 Comparison of various MagCOFs with other magnetic materials/adsorbents

Magnetic materials	Linear range (ng mL^{-1})	Limit of detection (ng mL^{-1})	Sample	Extraction time (min)	Recoveries (%)	Ref.
Endocrine disrupting chemicals						
Fe_3O_4@MIP	0.5–100	0.1–0.3	Canned orange/milk	3	72–113	164
magG@PDA@Zr-MOF	50–20 000	0.1–1	Water	20	64.8–92.8	165
Fe_3O_4@C	0.01–100	0.017–0.15	Tap water	20	47.9–119	166
Fe_3O_4@rGO	2.5–100	1.23	Tap water/river water/waste water	n.d.	96.3–112.6	167
Fe_3O_4@COFs	0.5–1000	0.08–0.21	Tea drinks	30	81.3–118.0	168
Ni@Fe_2O_4@COF	0.1–200	0.019–0.096	Tap/barrelled/river water; activated beverage; human urine/serum sample	5	83.4–106.2	159
Fe_3O_4@COFs	0.1–50	0.001–0.078	Human serum	10	93.0–107.8	70
Persistent organic pollutants						
Graphene/Fe_3O_4 composite	0.03–80	0.009–0.020	Water	4	83–107	169
Fe_3O_4@ZIF-8	1.0–100	0.08–0.24	Water	8	85.6–103.6	170
Magnetic MIL-100(Fe)	0.5–500	0.032–2.11	Water	10	81.4–126.9	171
PFu/Fe_3O_4	0.02–200	0.005–0.02	Urine samples	15	93.2–99.2	172
Magnetic TpPa-1	0.002–0.2	0.00024–0.00101	Water	n.d.	73–110	71
Sulfonamides Extraction						
$CoFe_2O_4$-graphene nanocomposite	20–50 000	1.59	Milk	20	62.0–104.3	173
Graphene-Fe_3O_4 nanoparticles	5–200	0.89–2.31	Milk	15	62.7–104.8	174
Fe_3O_4@GO	2.0–100	0.02–0.13	Milk	5	73.4–97.4	
Polypyrrole/SiO_2/Fe_3O_4 nanoparticles	0.30–200	0.30–1	Water	20	86.7–99.7	175
Fe_3O_4@COFs	1–500	0.2–1.0	Water, milk, pork, chicken, shrimp	20	65.3–107.3	114
Fe_3O_4@COF@Au-β-CD	2–100	0.8–1.6	Meat	30	78.9–112.0	150
Metal ion extraction						
Magnetic materials	Maximum adsorption capacity (mg g^{-1})					
Fe_3O_4@SiO_2	148.8					176
γ-Fe_2O_3@CTF-1	165.8					177
MPTS-mesoporous Fe_3O_4/C@SiO_2	118.6					178
Fe_3O_4@SiO_2-NH_2	27.2					179
M-DAPS50-COF-SH	383					131
Fe_3O_4@TpPa-1	246.45					153

properties. Although, COFs have achieved remarkable advances in separation applications but some crucial challenges are still to be addressed such as high cost, cumbersome filtration and centrifugation technique for the recovery of the adsorbent. Immobilization of COFs over MNPs has opened up a new avenue for the development of green and sustainable magnetic adsorbents by eliminating the shortcoming of traditionally used COFs. This review article presents an overview on the preparation of MagCOFs and their applicability in the extraction of various chemical pollutants, heavy metal ions, nitro explosives, *etc.* The combination of MNPs and COFs offered improved characteristics such as easy magnetic recovery, enhanced functionality, cost-effectiveness and high extraction efficiency. The incorporation of magnetism in COFs has been proven to be an effective strategy to solve the problem of recovery of COFs. Adsorption and recyclability are the key advantages of MagCOF materials. In addition, MagCOF-based adsorbents are being designed to selectively extract EDCs, POPs, PAHs, metal ions and even marine biotoxins. Usually, there are strong π–π stacking interactions, electrostatic interaction, hydrophobic effect and hydrogen bonding between phenyl rings of MagCOFs and benzene rings of the concerned analyte, thereby allowing efficient extraction/adsorption. Meanwhile, the present review gives new insights into the facile functional modification of COFs as adsorbent in MSPE. Hence, MagCOF based adsorbent opens a new door with a plethora of potential applications.

However, despite the promising results, the full potential of the MagCOFs composites in certain areas of concerns still need further improvement Besides, not only the extraction of EDCs, POPs, PAHs and metal ions, extraction of microorganisms will also need to be studied to fully open up their application as versatile adsorbent. Moreover, systematic and continuous efforts are required for better designing and large-scale applications of MagCOFs in various fields. In the next step, it is also necessary to gain insights about the toxicity of the nanomaterials for their long-term use. Another important point to consider is the better understanding of adsorption–desorption mechanism *i.e.* to avoid the use of non-green and costly solvents. Other aspect, which is of utmost importance is the synthetic cost and efficiency of the MagCOF composites. The use of high cost monomers to synthesize COFs materials is not economical. Therefore, to enhance manufacturing efficiency by reducing the monomers cost through incorporating cost-effective functional groups is a significant topic from future perspective. Also, large-scale magnetic separation of EDCs, marine bio-toxins, PPCPs, POPs, *etc.* from large amount of crude culture media at standard conditions is still required. In terms of extraction applications, MagCOFs materials have shown enhanced performance but the use of MagCOFs in catalysis and other applications is still in its infancy. Therefore, there is need to expand the scope of application. Also, due to presence of stable π–π stacking between COF layers, it can greatly improve the photocatalytic reactions. But it is believed that post-synthetic modification at the pore will provide opportunities for incorporation of specific active sites for catalysis.

Despite these above-mentioned challenges, undoubtedly, the progress in recent years have predicted well for the bright future of this new type of porous materials and we sincerely hope that the present review will significantly contribute in facilitating that development in near future.

Conflicts of interest

The authors declare no competing financial interest.

Acknowledgements

References

1 S.-Y. Ding and W. Wang, *Chem. Soc. Rev.*, 2013, **42**, 548–568.

2 X. Feng, X. Ding and D. Jiang, *Chem. Soc. Rev.*, 2012, **41**, 6010–6022.

3 R. K. Sharma, P. Yadav, M. Yadav, R. Gupta, P. Rana, A. Srivastava, R. Zbořil, R. S. Varma, M. Antonietti and M. B. Gawande, *Mater. Horiz.*, 2020, **7**, 411–454.

4 D. Ma, Y. Wang, A. Liu, S. Li, C. Lu and C. Chen, *Catalysts*, 2018, **8**, 404.

5 X. Guan, F. Chen, Q. Fang and S. Qiu, *Chem. Soc. Rev.*, 2020, **49**, 1357–1384.

6 A. Côté, *Science*, 2005, **310**, 1166.

7 J. L. Segura, M. J. Mancheño and F. Zamora, *Chem. Soc. Rev.*, 2016, **45**, 5635–5671.

8 C. S. Diercks and O. M. Yaghi, *Science*, 2017, **355**, eaal1585.

9 N. Huang, P. Wang and D. Jiang, *Nat. Rev. Mater.*, 2016, **1**, 1–19.

10 J. J. Jarju, A. M. Lavender, B. Espiña, V. Romero and L. M. Salonen, *Molecules*, 2020, **25**, 5404.

11 H. Hu, Q. Yan, R. Ge and Y. Gao, *Chin. J. Catal.*, 2018, **39**, 1167–1179.

12 Z. Wang, S. Zhang, Y. Chen, Z. Zhang and S. Ma, *Chem. Soc. Rev.*, 2020, **49**, 708–735.

13 S. Das, J. Feng and W. Wang, *Ann. Rev. Chem. Biomol. Eng.*, 2020, **11**, 131–153.

14 C. Y. Lin, L. Zhang, Z. Zhao and Z. Xia, *Adv. Mater.*, 2017, **29**, 1606635.

15 C. Y. Lin, D. Zhang, Z. Zhao and Z. Xia, *Adv. Mater.*, 2018, **30**, 1703646.

16 S. B. Alahakoon, C. M. Thompson, G. Occhialini and R. A. Smaldone, *ChemSusChem*, 2017, **10**, 2116–2129.

17 C. R. DeBlase, K. E. Silberstein, T.-T. Truong, H. C. D. Abruña and W. R. Dichtel, *J. Am. Chem. Soc.*, 2013, **135**, 16821–16824.

18 Z. Li, X. Feng, Y. Zou, Y. Zhang, H. Xia, X. Liu and Y. Mu, *Chem. Commun.*, 2014, **50**, 13825–13828.

19 Y. Zeng, R. Zou and Y. Zhao, *Adv. Mater.*, 2016, **28**, 2855–2873.

20 Y. Yusran, H. Li, X. Guan, Q. Fang and S. Qiu, *EnergyChem*, 2020, 100035.

21 Y. Han, M. Zhang, Y.-Q. Zhang and Z.-H. Zhang, *Green Chem.*, 2018, **20**, 4891–4900.

22 S.-Y. Ding, J. Gao, Q. Wang, Y. Zhang, W.-G. Song, C.-Y. Su and W. Wang, *J. Am. Chem. Soc.*, 2011, **133**, 19816–19822.

23 H. Xu, J. Gao and D. Jiang, *Nat. Chem.*, 2015, **7**, 905–912.

24 R. S. Gonçalves, A. B. de Oliveira, H. C. Sindra, B. S. Archanjo, M. E. Mendoza, L. S. Carneiro, C. D. Buarque and P. M. Esteves, *ChemCatChem*, 2016, **8**, 743–750.

25 D. Mullangi, S. Nandi, S. Shalini, S. Sreedhala, C. P. Vinod and R. Vaidhyanathan, *Sci. Rep.*, 2015, **5**, 10876.

26 A. K. Mandal, J. Mahmood and J. B. Baek, *ChemNanoMat*, 2017, **3**, 373–391.

27 L. Ma, S. Wang, X. Feng and B. Wang, *Chin. Chem. Lett.*, 2016, **27**, 1383–1394.

28 C. Zhang, S. Zhang, Y. Yan, F. Xia, A. Huang and Y. Xian, *ACS Appl. Mater. Interfaces*, 2017, **9**, 13415–13421.

29 H.-L. Qian, C. Dai, C.-X. Yang and X.-P. Yan, *ACS Appl. Mater. Interfaces*, 2017, **9**, 24999–25005.

30 Q. Fang, J. Wang, S. Gu, R. B. Kaspar, Z. Zhuang, J. Zheng, H. Guo, S. Qiu and Y. Yan, *J. Am. Chem. Soc.*, 2015, **137**, 8352–8355.

31 L. Bai, S. Z. F. Phua, W. Q. Lim, A. Jana, Z. Luo, H. P. Tham, L. Zhao, Q. Gao and Y. Zhao, *Chem. Commun.*, 2016, **52**, 4128–4131.

32 H. Zhao, Z. Jin, H. Su, X. Jing, F. Sun and G. Zhu, *Chem. Commun.*, 2011, **47**, 6389–6391.

33 N. Huang, L. Zhai, H. Xu and D. Jiang, *J. Am. Chem. Soc.*, 2017, **139**, 2428–2434.

34 N. Li, J. Du, D. Wu, J. Liu, N. Li, Z. Sun, G. Li and Y. Wu, *TrAC, Trends Anal. Chem.*, 2018, **108**, 154–166.

35 M. Gao, Q. Fu, M. Wang, K. Zhang, J. Zeng, L. Wang, Z. Xia and D. Gao, *Anal. Chim. Acta*, 2019, **1084**, 21–32.

36 D. Jiang, T. Hu, H. Zheng, G. Xu and Q. Jia, *Chem. – Eur. J.*, 2018, **24**, 10390–10396.

37 D. Li, M. He, B. Chen and B. Hu, *J. Chromatogr. A*, 2019, **1601**, 1–8.

38 Z.-D. Du, Y.-Y. Cui, C.-X. Yang and X.-P. Yan, *Talanta*, 2020, **206**, 120179.

39 M. Wierucka and M. Biziuk, *TrAC, Trends Anal. Chem.*, 2014, **59**, 50–58.

40 M. Safarikova and I. Safarik, *Biomagn. Res. Technol.*, 2004, **2**, 7.

41 Y. Chen and Z. Chen, *Talanta*, 2017, **165**, 188–193.

42 R. K. Sharma, S. Dutta, S. Sharma, R. Zbořil, R. S. Varma and M. B. Gawande, *Green Chem.*, 2016, **18**, 3184–3209.

43 Y. Monga, P. Kumar, R. K. Sharma, J. Filip, R. S. Varma, R. Zbořil and M. B. Gawande, *ChemSusChem*, 2020, **13**, 3288–3305.

44 G. Arora, M. Yadav, R. Gaur, R. Gupta and R. K. Sharma, *ChemistrySelect*, 2017, **2**, 10871–10879.

45 G. Arora, M. Yadav, R. Gaur, R. Gupta, P. Rana, P. Yadav and R. K. Sharma, *RSC Adv.*, 2020, **10**, 19390–19396.

46 P. Yadav, M. Yadav, R. Gaur, R. Gupta, G. Arora, P. Rana, A. Srivastava and R. K. Sharma, *ChemCatChem*, 2020, **12**, 2488–2496.

47 R. K. Sharma, M. Yadav and M. B. Gawande, *Ferrites and Ferrates: Chemistry and Applications in Sustainable Energy and Environmental Remediation*, ACS Publications, 2016, pp. 1–38.

48 K. J. Datta, A. K. Rathi, P. Kumar, J. Kaslik, I. Medrik, V. Ranc, R. S. Varma, R. Zbořil and M. B. Gawande, *Sci. Rep.*, 2017, **7**, 1–12.

49 S. Sá, M. B. Gawande, A. Velhinho, J. P. Veiga, N. Bundaleski, J. Trigueiro, A. Tolstogouzov, O. M. Teodoro, R. Zbořil and R. S. Varma, *Green Chem.*, 2014, **16**, 3494–3500.

50 M. B. Gawande, A. K. Rathi, P. S. Branco and R. S. Varma, *Appl. Sci.*, 2013, **3**, 656–674.

51 M. B. Gawande, A. K. Rathi, I. D. Nogueira, R. S. Varma and P. S. Branco, *Green Chem.*, 2013, **15**, 1895–1899.

52 M. B. Gawande, V. D. Bonifácio, R. S. Varma, I. D. Nogueira, N. Bundaleski, C. A. A. Ghumman, O. M. Teodoro and P. S. Branco, *Green Chem.*, 2013, **15**, 1226–1231.

53 M. B. Gawande, P. S. Branco and R. S. Varma, *Chem. Soc. Rev.*, 2013, **42**, 3371–3393.

54 R. Gupta, M. Yadav, R. Gaur, G. Arora, P. Yadav and R. K. Sharma, *Mater. Horiz.*, 2020, **7**, 3097–3130.

55 G. Arora, M. Yadav, R. Gaur, R. Gupta, P. Yadav, R. Dixit and R. K. Sharma, *Nanoscale*, 2021, **13**, 10967–11003.

56 Y. Wang, S. Wu, D. Wu, J. Shen, Y. Wei and C. Wang, *Anal. Chim. Acta*, 2020, **1093**, 61–74.

57 Y. Zhang, Y. Song, J. Wu, R. Li, D. Hu, Z. Lin and Z. Cai, *Chem. Commun.*, 2019, **55**, 3745–3748.

58 Y. Liao, J. Li and A. Thomas, *ACS Macro Lett.*, 2017, **6**, 1444–1450.

59 N. Li, D. Wu, N. Hu, G. Fan, X. Li, J. Sun, X. Chen, Y. Suo, G. Li and Y. Wu, *J. Agric. Food Chem.*, 2018, **66**, 3572–3580.

60 G. Lin, C. Gao, Q. Zheng, Z. Lei, H. Geng, Z. Lin, H. Yang and Z. Cai, *Chem. Commun.*, 2017, **53**, 3649–3652.

61 J. Liu, G. Li, D. Wu, Y. Yu, J. Chen and Y. Wu, *Rapid Commun. Mass Spectrom.*, 2020, **34**, e8742.

62 Y. Xie, T. Zhang, Y. Chen, Y. Wang and L. Wang, *Talanta*, 2020, **213**, 120843.

63 D. Wei, J. Li, Z. Chen, L. Liang, J. Ma, M. Wei, Y. Ai and X. Wang, *J. Mol. Liq.*, 2020, **301**, 112431.

64 F.-F. Wu, Q.-Y. Chen, X.-J. Ma, T.-T. Li, L.-F. Wang, J. Hong, Y.-H. Sheng, M.-L. Ye and Y. Zhu, *Anal. Methods*, 2019, **11**, 3381–3387.

65 M. Zhang, J. Li, C. Zhang, Z. Wu, Y. Yang, J. Li, F. Fu and Z. Lin, *J. Chromatogr. A*, 2019, 460773.

66 J. Lu, R. Wang, J. Luan, Y. Li, X. He, L. Chen and Y. Zhang, *J. Chromatogr. A*, 2020, 460898.

67 Y. Li, C.-X. Yang and X.-P. Yan, *Chem. Commun.*, 2017, **53**, 2511–2514.

68 R. Gupta, G. Arora, P. Yadav, R. Dixit, A. Srivastava and R. K. Sharma, *Dalton Trans.*, 2021, **50**, 890–898.

69 Z.-D. Du, Y.-Y. Cui, C.-X. Yang and X.-P. Yan, *ACS Appl. Nano Mater.*, 2019, **2**, 1232–1241.

70 L. Chen, Y. He, Z. Lei, C. Gao, Q. Xie, P. Tong and Z. Lin, *Talanta*, 2018, **181**, 296–304.

71 S. He, T. Zeng, S. Wang, H. Niu and Y. Cai, *ACS Appl. Mater. Interfaces*, 2017, **9**, 2959–2965.

72 G. Li, A. Wen, J. Liu, D. Wu and Y. Wu, *Food Chem.*, 2021, **337**, 127974.

73 J. Liu, N. Wang and L. Ma, *Chem. – Asian J.*, 2020, **15**, 338–351.

74 S. M. Rogge, A. Bavykina, J. Hajek, H. Garcia, A. I. Olivos-Suarez, A. Sepúlveda-Escribano, A. Vimont, G. Clet, P. Bazin and F. Kapteijn, *Chem. Soc. Rev.*, 2017, **46**, 3134–3184.

75 V. Romero, S. P. Fernandes, L. Rodriguez-Lorenzo, Y. V. Kolen'ko, B. Espiña and L. M. Salonen, *Nanoscale*, 2019, **11**, 6072–6079.

76 M. He, Q. Liang, L. Tang, Z. Liu, B. Shao, Q. He, T. Wu, S. Luo, Y. Pan, C. Zhao, C. Niu and Y. Hu, *Coord. Chem. Rev.*, 2021, **449**, 214219.

77 C. Casals-Casas and B. Desvergne, *Ann. Rev. Physiol.*, 2011, **73**, 135–162.

78 R. Gupta, P. Kumar, N. Fahmi, B. Garg, S. Dutta, S. Sachar, A. S. Matharu and K. S. Vimaleswaran, *Curr. Res. Green Sustainable Chem.*, 2020, **3**, 100009.

79 B. Blumberg, T. Iguchi and A. Odermatt, *J. Steroid Biochem. Mol. Biol.*, 2011, **127**, 1–3.

80 Z.-H. Deng, X. Wang, X.-L. Wang, C.-L. Gao, L. Dong, M.-L. Wang and R.-S. Zhao, *Microchim. Acta*, 2019, **186**, 108.

81 C. Tan, J. Li, W. Liu, Q. Zhao, X. Wang and Y. Li, *Chem. Eng. J.*, 2020, 125191.

82 J. R. Rochester, *Reprod. Toxicol.*, 2013, **42**, 132–155.

83 V. Mustieles, R. Pérez-Lobato, N. Olea and M. F. Fernández, *Neurotoxicology*, 2015, **49**, 174–184.

84 I. Bautista-Toledo, M. Ferro-García, J. Rivera-Utrilla, C. Moreno-Castilla and F. Vegas Fernández, *Environ. Sci. Technol.*, 2005, **39**, 6246–6250.

85 R. Risebrough, P. Rieche, D. Peakall, S. T. Herman and M. Kirven, *Nature*, 1968, **220**, 1098–1102.

86 S. H. Safe, *Crit. Rev. Toxicol.*, 1994, **24**, 87–149.

87 R. Tehrani and B. Van Aken, *Environ. Sci. Pollut. Res.*, 2014, **21**, 6334–6345.

88 R. Gupta, M. Yadav, R. Gaur, G. Arora and R. K. Sharma, *Green Chem.*, 2017, **19**, 3801–3812.

89 M. B. Gawande, Y. Monga, R. Zbořil and R. K. Sharma, *Coord. Chem. Rev.*, 2015, **288**, 118–143.

90 R. Gupta, M. Yadav, R. Gaur, G. Arora, P. Rana, P. Yadav, A. Adholeya and R. K. Sharma, *ACS Omega*, 2019, **4**, 21529–21539.

91 P. Rana, R. Gaur, R. Gupta, G. Arora, A. Jayashree and R. K. Sharma, *Chem. Commun.*, 2019, **55**, 7402–7405.

92 R. K. Sharma, R. Gaur, M. Yadav, A. Goswami, R. Zbořil and M. B. Gawande, *Sci. Rep.*, 2018, **8**, 1–12.

93 R. K. Sharma, M. Yadav, Y. Monga, R. Gaur, A. Adholeya, R. Zbořil, R. S. Varma and M. B. Gawande, *ACS Sustainable Chem. Eng.*, 2016, **4**, 1123–1130.

94 R. K. Sharma, M. Yadav, R. Gaur, Y. Monga and A. Adholeya, *Catal. Sci. Technol.*, 2015, **5**, 2728–2740.

95 R. K. Sharma, R. Gaur, M. Yadav, A. K. Rathi, J. Pechousek, M. Petr, R. Zbořil and M. B. Gawande, *ChemCatChem*, 2015, **7**, 3495–3502.

96 H. I. Abdel-Shafy and M. S. Mansour, *Egypt. J. Pet.*, 2016, **25**, 107–123.

97 R. Wang and Z. Chen, *Microchim. Acta*, 2017, **184**, 3867–3874.

98 M. Kahle, I. J. Buerge, A. Hauser, M. D. Muller and T. Poiger, *Environ. Sci. Technol.*, 2008, **42**, 7193–7200.

99 X. Lv, L. Pan, J. Wang, L. Lu, W. Yan, Y. Zhu, Y. Xu, M. Guo and S. Zhuang, *Environ. Pollut.*, 2017, **222**, 504–512.

100 Y. Li, H. Zhang, Y. Chen, L. Huang, Z. Lin and Z. Cai, *ACS Appl. Mater. Interfaces*, 2019, **11**, 22492–22500.

101 A. J. Ebele, M. A.-E. Abdallah and S. Harrad, *Emerging Cont.*, 2017, **3**, 1–16.

102 R. U. Halden, *Environ. Sci. Technol.*, 2014, **48**, 3603–3611.

103 R. U. Halden and D. H. Paull, *Environ. Sci. Technol.*, 2005, **39**, 1420–1426.

104 C. P. Higgins, Z. J. Paesani, T. E. Abbott Chalew, R. U. Halden and L. S. Hundal, *Environ. Toxicol. Chem.*, 2011, **30**, 556–563.

105 Z. Sun, W. Schüssler, M. Sengl, R. Niessner and D. Knopp, *Anal. Chim. Acta*, 2008, **620**, 73–81.

106 N. Mao, L. Huang and Q. Shuai, *ACS Omega*, 2019, **4**, 15051–15060.

107 L. Huang, N. Mao, Q. Yan, D. Zhang and Q. Shuai, *ACS Appl. Nano Mater.*, 2019, **3**, 319–326.

108 S. Zhuang, R. Chen, Y. Liu and J. Wang, *J. Hazard. Mater.*, 2020, **385**, 121596.

109 E. K. Rowinsky and R. C. Donehower, *N. Engl. J. Med.*, 1995, **332**, 1004–1014.

110 M. C. Wani, H. L. Taylor, M. E. Wall, P. Coggon and A. T. McPhail, *J. Am. Chem. Soc.*, 1971, **93**, 2325–2327.

111 V. Walsh and J. Goodman, *Soc. Sci. Med.*, 1999, **49**, 1215–1225.

112 A. Scozzafava, T. Owa, A. Mastrolorenzo and C. T. Supuran, *Curr. Med. Chem.*, 2003, **10**, 925–953.

113 H. Wu, Y. Shi, X. Guo, S. Zhao, J. Du, H. Jia, L. He and L. Du, *J. Sep. Sci.*, 2016, **39**, 4398–4407.

114 J. Zhang, Z. Chen, S. Tang, X. Luo, J. Xi, Z. He, J. Yu and F. Wu, *Anal. Chim. Acta*, 2019, **1089**, 66–77.

115 Y. Yang, G. Li, D. Wu, A. Wen, Y. Wu and X. Zhou, *Microchim. Acta*, 2020, **187**, 278.

116 P. M. Rudd, T. Elliott, P. Cresswell, I. A. Wilson and R. A. Dwek, *Science*, 2001, **291**, 2370–2376.

117 J. N. Arnold, M. R. Wormald, R. B. Sim, P. M. Rudd and R. A. Dwek, *Annu. Rev. Immunol.*, 2007, **25**, 21–50.

118 K. Ohtsubo and J. D. Marth, *Cell*, 2006, **126**, 855–867.

119 H. Wang, F. Jiao, F. Gao, J. Huang, Y. Zhao, Y. Shen, Y. Zhang and X. Qian, *J. Mater. Chem. B*, 2017, **5**, 4052–4059.

120 Y. Wu, N. Sun and C. Deng, *ACS Appl. Mater. Interfaces*, 2020, **12**, 9814–9823.

121 B. Luo, L. Yu, J. He, Z. Li, F. Lan and Y. Wu, *J. Chromatogr. B*, 2020, 122080.

122 F. Xiong, L. Jiang and Q. Jia, *Anal. Chim. Acta*, 2020, **1099**, 103–110.

123 F. Ding, Y. Zhao, H. Liu and W. Zhang, *Analyst*, 2020, **145**, 4341–4351.

124 T. Yasumoto and M. Murata, *Chem. Rev.*, 1993, **93**, 1897–1909.

125 L. M. Salonen, S. R. Pinela, S. P. Fernandes, J. Louçano, E. Carbó-Argibay, M. P. Sarriá, C. Rodríguez-Abreu, J. Peixoto and B. Espiña, *J. Chromatogr. A*, 2017, **1525**, 17–22.

126 R. K. Sharma, M. Yadav and R. Gupta, *Chemistry and Water*, Elsevier, 2017, pp. 183–205.

127 M. Yadav, R. Gupta and R. K. Sharma, *Advances in Water Purification Techniques*, Elsevier, 2019, pp. 355–383.

128 R. K. Sharma, A. Puri, Y. Monga and A. Adholeya, *J. Mater. Chem. A*, 2014, **2**, 12888–12898.

129 R. K. Sharma, H. Kumar and A. Kumar, *RSC Adv.*, 2015, **5**, 43371–43380.

130 C. T. Driscoll, R. P. Mason, H. M. Chan, D. J. Jacob and N. Pirrone, *Environ. Sci. Technol.*, 2013, **47**, 4967–4983.

131 L. Huang, R. Shen, R. Liu and Q. Shuai, *J. Hazard. Mater.*, 2020, **392**, 122320.

132 M. Costa, *Crit. Rev. Toxicol.*, 1997, **27**, 431–442.

133 X. Zhong, Z. Lu, W. Liang and B. Hu, *J. Hazard. Mater.*, 2020, **393**, 122353.

134 M. Rong, L. Lin, X. Song, T. Zhao, Y. Zhong, J. Yan, Y. Wang and X. Chen, *Anal. Chem.*, 2015, **87**, 1288–1296.

135 M. Wang, M. Gao, L. Deng, X. Kang, K. Zhang, Q. Fu, Z. Xia and D. Gao, *Microchem. J.*, 2020, **154**, 104590.

136 S. Safe, *Toxicol. Sci.*, 2000, **56**, 251–252.

137 A. Chao, M. J. Thun, E. J. Jacobs, S. J. Henley, C. Rodriguez and E. E. Calle, *J. Natl. Cancer Inst.*, 2000, **92**, 1888–1896.

138 S. S. Hecht, *Nat. Rev. Cancer*, 2003, **3**, 733–744.

139 Y. Chen, W. Zhang, Y. Zhang, Z. Deng, W. Zhao, H. Du, X. Ma, D. Yin, F. Xie and Y. Chen, *J. Chromatogr. A*, 2018, **1556**, 1–9.

140 C. A. Staples, D. R. Peterson, T. F. Parkerton and W. J. Adams, *Chemosphere*, 1997, **35**, 667–749.

141 F. L. Mayer, D. L. Stalling and J. L. Johnson, *Nature*, 1972, **238**, 411–413.

142 Y.-H. Pang, Q. Yue, Y.-Y. Huang, C. Yang and X.-F. Shen, *Talanta*, 2020, **206**, 120194.

143 Y. Yan, Y. Lu, B. Wang, Y. Gao, L. Zhao, H. Liang and D. Wu, *ACS Appl. Mater. Interfaces*, 2018, **10**, 26539–26545.

144 S. Zereshki, P. Daraei and A. Shokri, *J. Hazard. Mater.*, 2018, **356**, 1–8.

145 A. Martelli, G. B. Campart, R. Canonero, R. Carrozzino, F. Mattioli, L. Robbiano and M. Cavanna, *Mutat. Res., Genet. Toxicol. Environ. Mutagen.*, 1998, **414**, 37–47.

146 J. Rochat, P. Demenge and J. Rerat, *Toxicol. Eur. Res.*, 1978, **1**, 23–26.

147 S. Shakeri, Z. Rafiee and K. Dashtian, *J. Chem. Eng. Data*, 2020, **65**, 696–705.

148 Z.-H. Deng, X. Wang, X.-L. Wang, C.-L. Gao, L. Dong, M.-L. Wang and R.-S. Zhao, *Microchim. Acta*, 2019, **186**, 108.

149 L. Huang, N. Mao, Q. Yan, D. Zhang and Q. Shuai, *ACS Appl. Nano Mater.*, 2020, **3**, 319–326.

150 Y. Yang, G. Li, D. Wu, A. Wen, Y. Wu and X. Zhou, *Microchim. Acta*, 2020, **187**, 278.

151 M. Wang, M. Gao, L. Deng, X. Kang, K. Zhang, Q. Fu, Z. Xia and D. Gao, *Microchem. J.*, 2020, **154**, 104590.

152 V. Romero, S. P. S. Fernandes, L. Rodriguez-Lorenzo, Y. V. Kolen'ko, B. Espiña and L. M. Salonen, *Nanoscale*, 2019, **11**, 6072–6079.

153 X. Zhong, Z. Lu, W. Liang and B. Hu, *J. Hazard. Mater.*, 2020, **393**, 122353.

154 A. Wen, G. Li, D. Wu, Y. Yu, Y. Yang, N. Hu, H. Wang, J. Chen and Y. Wu, *J. Chromatogr. A*, 2020, **1612**, 460651.

155 L. Chen, M. Zhang, F. Fu, J. Li and Z. Lin, *J. Chromatogr. A*, 2018, **1567**, 136–146.

156 A. Smith, P. M. Pennefather, S. B. Kaye and C. A. Hart, *Drugs*, 2001, **61**, 747–761.

157 G. G. Zhanel, K. Ennis, L. Vercaigne, A. Walkty, A. S. Gin, J. Embil, H. Smith and D. J. Hoban, *Drugs*, 2002, **62**, 13–59.

158 M. Wang, M. Gao, K. Zhang, L. Wang, W. Wang, Q. Fu, Z. Xia and D. Gao, *Microchim. Acta*, 2019, **186**, 827.

159 C. Tan, J. Li, W. Liu, Q. Zhao, X. Wang and Y. Li, *Chem. Eng. J.*, 2020, **396**, 125191.

160 R. Wang and Z. Chen, *Microchim. Acta*, 2017, **184**, 3867–3874.

161 Y. Chen, W. Zhang, Y. Zhang, Z. Deng, W. Zhao, H. Du, X. Ma, D. Yin, F. Xie, Y. Chen and S. Zhang, *J. Chromatogr. A*, 2018, **1556**, 1–9.

162 H. L. de Oliveira, L. S. Teixeira, L. A. F. Dinali, B. C. Pires, N. S. Simões and K. B. Borges, *Microchem. J.*, 2019, **150**, 104162.

163 L. Ciofi, D. Fibbi, U. Chiuminatto, E. Coppini, L. Checchini and M. Del Bubba, *J. Chromatogr. A*, 2013, **1283**, 53–61.

164 Z. Xu, L. Ding, Y. Long, L. Xu, L. Wang and C. Xu, *Anal. Methods*, 2011, **3**, 1737–1744.

165 X. Wang and C. Deng, *Talanta*, 2015, **144**, 1329–1335.

166 Z. Huang and H. K. Lee, *J. Chromatogr. A*, 2015, **1414**, 41–50.

167 E. Ö. Er, A. Çağlak, G. Ö. Engin and S. Bakirdere, *Microchem. J.*, 2019, **146**, 423–428.

168 Z.-H. Deng, X. Wang, X.-L. Wang, C.-L. Gao, L. Dong, M.-L. Wang and R.-S. Zhao, *Microchim. Acta*, 2019, **186**, 108.

169 A. Mehdinia, N. Khodaee and A. Jabbari, *Anal. Chim. Acta*, 2015, **868**, 1–9.

170 X. Liu, Z. Sun, G. Chen, W. Zhang, Y. Cai, R. Kong, X. Wang, Y. Suo and J. You, *J. Chromatogr. A*, 2015, **1409**, 46–52.

171 F. Du, Q. Qin, J. Deng, G. Ruan, X. Yang, L. Li and J. Li, *J. Sep. Sci.*, 2016, **39**, 2356–2364.

172 A. Amiri, M. Baghayeri and M. Kashmari, *Microchim. Acta*, 2016, **183**, 149–156.

173 Y. Li, X. Wu, Z. Li, S. Zhong, W. Wang, A. Wang and J. Chen, *Talanta*, 2015, **144**, 1279–1286.

174 Z. Li, Y. Li, M. Qi, S. Zhong, W. Wang, A.-J. Wang and J. Chen, *J. Sep. Sci.*, 2016, **39**, 3818–3826.

175 T. Sukchuay, P. Kanatharana, R. Wannapob, P. Thavarungkul and O. Bunkoed, *J. Sep. Sci.*, 2015, **38**, 3921–3927.

176 S. Zhang, Y. Zhang, J. Liu, Q. Xu, H. Xiao, X. Wang, H. Xu and J. Zhou, *Chem. Eng. J.*, 2013, **226**, 30–38.

177 K. Leus, K. Folens, N. R. Nicomel, J. P. H. Perez, M. Filippousi, M. Meledina, M. M. Dîrtu, S. Turner, G. Van Tendeloo, Y. Garcia, G. Du Laing and P. Van Der Voort, *J. Hazard. Mater.*, 2018, **353**, 312–319.

178 X. Zhang, T. Wu, Y. Zhang, D. H. L. Ng, H. Zhao and G. Wang, *RSC Adv.*, 2015, **5**, 51446–51453.

179 S. Shi, J. Yang, S. Liang, M. Li, Q. Gan, K. Xiao and J. Hu, *Sci. Total Environ.*, 2018, **628–629**, 499–508.